





## TOOLBOX OPEN ACCESS

# A Sensitive and Versatile Cell-Based Assay Combines Luminescence and Trapping Approaches to Monitor Unconventional Protein Secretion

Morgane Denus<sup>1</sup> | Aurore Filaquier<sup>1</sup> | William Fargues<sup>1</sup>  | Eloïse Néel<sup>1</sup> | Sarah E. Stewart<sup>2</sup> | Maëlle Colladant<sup>1</sup> | Thomas Curel<sup>1</sup> | Alexandre Mezghrani<sup>3</sup>  | Philippe Marin<sup>1</sup>  | Sylvie Claeysen<sup>1</sup> | David C. Rubinsztein<sup>4,5</sup> | Marie-Laure Parmentier<sup>1</sup> | Julien Villeneuve<sup>1</sup> 

<sup>1</sup>Institute of Functional Genomics (IGF), University of Montpellier, CNRS, INSERM, Montpellier, France | <sup>2</sup>Department of Biochemistry and Chemistry, School of Agriculture, Biomedicine and Environment, La Trobe Institute for Molecular Science, La Trobe University, Melbourne, Victoria, Australia | <sup>3</sup>Centre de Biologie Structurale (CBS), University of Montpellier, CNRS, INSERM, Montpellier, France | <sup>4</sup>Department of Medical Genetics, University of Cambridge, Cambridge Institute for Medical Research, Cambridge, UK | <sup>5</sup>UK Dementia Research Institute, Cambridge, UK

**Correspondence:** Marie-Laure Parmentier ([marie-laure.parmontier@igf.cnrs.fr](mailto:marie-laure.parmontier@igf.cnrs.fr)) | Julien Villeneuve ([julien.villeneuve@igf.cnrs.fr](mailto:julien.villeneuve@igf.cnrs.fr))

**Received:** 6 December 2024 | **Revised:** 16 April 2025 | **Accepted:** 7 May 2025

**Funding:** This study was supported by the Centre National de la Recherche Scientifique (CNRS), the Institut National pour la Santé et la Recherche Médicale (INSERM), the Université de Montpellier, the Fondation Vaincre Alzheimer, the Association France Parkinson, the France Alzheimer et maladies apparentées, the Fédération pour la Recherche sur le Cerveau, the Fondation pour la Recherche Médicale (FRM) (MND202310017892), the Agence Nationale de la Recherche (ANR-23-CE16-0012) and (ANR-24-CE16-5161-02), the Centre of Excellence in Neurodegeneration (CoEN) of Montpellier, the Australian Research Council (DE200100611), the UK Dementia Research Institute (through UK DRI Ltd.), principally funded by the UK Medical Research Council and the National Institute for Health Research Cambridge Biomedical Research Centre at Addenbrooke's Hospital and the French National Research Agency (ANR-10-INBS-04, "Investments for the Future") (Biocampus, UM-CNRS-INSERM, Montpellier, France).

**Keywords:** intercellular communication | intracellular compartments | neurodegenerative diseases | protein trafficking | secretory pathway | split luciferase | tau | unconventional protein secretion

## ABSTRACT

In addition to the conventional endoplasmic reticulum (ER)-Golgi secretory pathway, alternative routes are increasingly recognized for their critical roles in exporting a growing number of secreted factors. These alternative processes, collectively referred to as unconventional protein secretion (UcPS), challenge traditional views of protein and membrane trafficking. Unlike the well-characterized molecular machinery of the conventional secretory pathway, the mechanisms underlying UcPS remain poorly understood. Various UcPS pathways may involve direct transport of cytosolic proteins across the plasma membrane or the incorporation of cargo proteins into intracellular compartments redirected for secretion. Identifying the specific chaperones, transporters and fusion machinery involved in UcPS cargo recognition, selection and transport is crucial to decipher how cargo proteins are selectively or synergistically directed through multiple secretory routes. These processes can vary depending on cell type and in response to particular stress conditions or cellular demands, underscoring the need for standardized tools and methods to study UcPS. Here, we combine the sensitivity of split NanoLuc Binary Technology with the versatility of the Retention Using Selective Hooks (RUSH) system to develop a straightforward and reliable cell-based assay for investigating both conventional and unconventional protein secretion. This system allows for the identification of intracellular compartments involved in UcPS cargo trafficking. Additionally, its sensitivity enabled us to demonstrate that disease-associated mutants or variants of Tau

Morgane Denus, Aurore Filaquier and William Fargues are joint first authors.

Marie-Laure Parmentier and Julien Villeneuve are joint last authors.

This is an open access article under the terms of the [Creative Commons Attribution-NonCommercial-NoDerivs](https://creativecommons.org/licenses/by-nc-nd/4.0/) License, which permits use and distribution in any medium, provided the original work is properly cited, the use is non-commercial and no modifications or adaptations are made.

© 2025 The Author(s). *Traffic* published by John Wiley & Sons Ltd.

and superoxide dismutase-1 (SOD1) show altered secretion via UcPS. Finally, we leveraged this assay to screen for Alzheimer's disease risk factors, revealing a functional link between amyloid-beta production and Tau UcPS. This robust assay provides a powerful tool for increasing our knowledge of protein secretion mechanisms in physiological and pathological contexts.

## 1 | Introduction

In eukaryotic cells, the mechanisms by which secreted factors reach the extracellular space to exert their biological functions are more diverse than originally thought. Indeed, the traditional view that all secreted proteins contain an N-terminal signal sequence that directs them through the endoplasmic reticulum (ER)–Golgi secretory pathway has been challenged by seminal discoveries [1–3]. These findings highlight the existence of “unconventional protein secretion” (UcPS), a set of processes that export outside the cells, numerous cytosolic proteins lacking a signal sequence for ER entry [4–10]. These include various inflammatory cytokines, annexins, heat shock proteins, lipid chaperones, galectins and aggregation-prone proteins, among others.

While it is tempting to hypothesize that UcPS is governed by common principles akin to the evolutionarily conserved ER–Golgi pathway [11], recent research indicates a higher level of diversity and heterogeneity within UcPS mechanisms and the existence of several UcPS routes. In Types I and II UcPS, proteins are directly translocated across the plasma membrane (PM) via protein channels and ABC transporters, respectively [12, 13]. In contrast, Type III UcPS involves the incorporation of cytosolic proteins into intracellular compartments such as autophagosomes, endosomes, multivesicular bodies (MVBs), or lysosomes, which are then redirected for secretion by acquiring exocytosis properties [14–19]. In some cases, Type III UcPS also triggers the formation of vesicular intermediates *de novo* in response to cellular stresses. A notable example is the biogenesis of the compartment for unconventional protein secretion (CUPS) in yeast under starvation conditions, which is crucial for the export of proteins such as *acb1*, SOD1 and thioredoxins. CUPS are composed of tubule-vesicular clusters that form and mature from pre-existing Golgi and endosomal membranes. In their immature state, CUPS resemble the mammalian ER–Golgi intermediate compartment (ERGIC). Once CUPS adopt their stable form, cargo proteins incorporated into the CUPS lumen are exported from this sorting station through mechanisms that remain to be fully characterized [20–25]. Additionally, in Type IV UcPS, ER-localized transmembrane proteins can bypass the Golgi apparatus and directly reach the PM [26, 27]. Cytosolic proteins can also be transported to neighboring cells through microvesicles or tunneling nanotubes (TNTs) generated at the PM [28–31]. Despite the diversity of UcPS mechanisms, common players and hubs are also emerging, suggesting the potential for a more unified understanding of these processes. Key players, such as the GRASP protein family and its orthologs, have been identified as crucial factors in the export of various cargo proteins through both Types III and IV UcPS across multiple organisms, from yeast to mammals [3, 20, 26, 32–34]. Lysosomes have also emerged as multifunctional organelles at the intersection of several intracellular trafficking pathways, serving as a convergence point for many cargo proteins in Type III UcPS and in TNT-mediated intercellular communication [9, 15, 19, 29, 35–39].

Despite the central role of UcPS in physiological and pathological conditions [36, 37, 40, 41], most of the underlying mechanisms remain poorly understood. Key challenges include unraveling the conserved and context-specific molecular mechanisms, identifying the regulatory factors that govern UcPS processes, and characterizing the amino acid motifs that direct cargo recognition and selection. Additionally, understanding how intracellular compartments are repurposed for secretion and exploring the evolutionary origins and adaptations of UcPS are crucial for advancing our knowledge in this field.

One major obstacle in studying UcPS is the relatively low amounts of secreted proteins compared to the total intracellular pool of the same protein. To circumvent this limitation, studies often extend the secretion period to 1–2 days. This can result in cell detachment, stress and cytosolic leakage, which can interfere with the detection of active UcPS processes. Current detection methods also face limitations. Techniques like Western blotting may lack sensitivity, while enzyme-linked immunosorbent assays (ELISAs) and homogeneous time resolved fluorescence (HTRF) assays can be expensive and require the use of specific high-affinity antibodies. Immunoprecipitation is time-consuming, and quantitative mass spectrometry is not scalable for high-throughput analysis. Here, we developed an assay for UcPS based on a luminescent reporter that combines high sensitivity, low cost, simplicity, versatility and scalability for high-throughput applications. Additionally, we incorporated a trapping approach to identify the compartments through which UcPS cargos transit for their export, with a particular focus on Type III UcPS. By applying this assay to a variety of cargos, including those trafficked via specific UcPS pathways and those linked to neurodegenerative diseases, we demonstrate its broad relevance and applicability. This new cell-based assay provides a powerful tool to address key challenges in the study of UcPS and offers new opportunities for understanding its role in both physiological and pathological contexts.

## 2 | Results

### 2.1 | A Quantitative Luminescent Assay to Monitor Conventional and Unconventional Protein Secretion

Using human SH-SY5Y neuroblastoma cells, we generated several lines stably expressing a specific cargo protein fused with the HiBit sequence. These cargo proteins included tumor necrosis factor- $\alpha$  (TNF $\alpha$ ), a proinflammatory cytokine containing an N-terminal signal sequence that is secreted via the conventional ER–Golgi pathway [42], as well as several proteins that lack a signal sequence for ER entry, which have been reported to be secreted via UcPS. These include fibroblast growth factor-2 (FGF2), the best-characterized example of Type I UcPS cargo protein [43], interleukin-1 $\beta$  (IL1 $\beta$ ) and galectin-3 (Gal3), which are all known to be secreted through

Types I and III UcPS [14, 41, 44, 45]. Additionally, we included three proteins associated with neurodegenerative diseases and secreted via Type III UcPS, namely  $\alpha$ -synuclein ( $\alpha$ SNC), superoxide dismutase-1 (SOD1) and Tau [37, 46, 47]. Recent studies suggested that Tau may also be secreted by Type I UcPS [48, 49]. A cell line expressing green fluorescent protein (GFP) fused to the HiBit sequence was also generated and used as a negative control. The HiBit tag, an 11-amino-acid peptide, has high affinity for its larger subunit, LgBit. Upon interaction, this reconstituted complex exhibits luciferase activity enabling split luciferase complementation assays [50] (Figure 1A,B). Each cargo protein was also fused with streptavidin-binding protein (SBP), allowing the use and adaptation of the Retention Using Selective Hooks (RUSH) system through streptavidin (Strep)–SBP interaction [51]. Western blotting of total cell lysates with an anti-HiBit antibody confirmed the correct expression of each cargo protein with the expected molecular weight migration shift, accounting for their fusion with the HiBit and SBP tags (Figure 1C). To monitor protein secretion, cells were incubated in complete medium for 12 h, followed by luciferase activity quantification in both cell lysates and media. The assay demonstrated high sensitivity, with a signal-to-noise ratio exceeding two logs for all cargo proteins (Figure 1D,E). Notably, in contrast to the high secretion efficiency of signal sequence-containing TNF $\alpha$  (282% of the total intracellular pool after 12 h), UcPS cargo proteins were released with much lower efficiency, ranging from 2.4% for IL1 $\beta$  to 5.3% for Tau (relative to their respective total intracellular pools after 12 h) (Figure S1). Kinetic experiments also revealed a time-dependent increase in luminescence in the culture media for all cargo proteins, except for GFP, which did not increase over time, demonstrating the assay's specificity (Figure 1F, upper panel). Importantly, the increase in extracellular luminescence was not due to cytosol leakage, as extracellular lactate dehydrogenase (LDH) activity remained unchanged (Figure 1F, bottom panel). The comparison of multiple UcPS cargos vs. GFP, combined with kinetic data and the lack of LDH release, confirmed that the developed assay can distinguish between active and specific UcPS-mediated secretion and non-specific protein release due to cell lysis or stress.

To further validate the assay, we examined the effect of brefeldin A (BFA), a chemical inhibitor of protein transport through the ER–Golgi membranes. BFA induces the fusion of Golgi membranes with the ER and endosomes, and the relocation of peripheral Golgi matrix proteins such as GM130 and GORASP2 to the ER exit site [52–54] (Figure 2A). As expected, BFA treatment reduced TNF $\alpha$  secretion, consistent with its transport via the conventional ER–Golgi pathway. In contrast, the secretion of UcPS cargos was unaffected (Figure 2B). Similar results were observed in cells with SCFD1 depletion (expression reduced to 24%), a factor with a key role for the transport of signal sequence-containing cargo proteins between the ER and the Golgi apparatus [55] (Figure 2C,D). However, it is important to note that recent studies have highlighted a greater overlap and shared factors between UcPS and the conventional ER–Golgi secretory pathway than previously recognized, indicating that these processes are not completely independent. For example, the central role of the ERGIC compartment in the TMED10-channelled UcPS (THU) pathway [56, 57], as well as the involvement of endo/lysosomal compartments in the secretion of both

UcPS cargos and signal sequence-containing cargo proteins, exemplify this interconnection [9]. In this context, the lack of a significant effect from genetic or pharmacologic inhibition of the ER–Golgi secretory pathway on UcPS can likely be explained by the fact that, under our experimental conditions, the blockage of this pathway is not complete. This is evidenced by the residual secretion of TNF $\alpha$  observed even after BFA treatment or SCFD1 knockdown (Figure 2B,D). This partial inhibition may still allow for the secretion of very low amounts of UcPS cargo (Figure S1), as it likely provides sufficient factors or machinery required for UcPS.

Given that UcPS cargo proteins can be released into the extracellular space either in free form or enclosed within extracellular vesicles [45–47, 58], we sought to determine whether our split luciferase complementation assay could distinguish between these different secreted forms. The cell-conditioned medium was collected after 12 h and incubated with or without digitonin, a detergent used to permeabilize membranes. In the absence of digitonin, only the free form of the protein is quantified. In the presence of digitonin, vesicle-enclosed reporters become accessible to LgBit, allowing the measurement of the total amount of secreted protein. The addition of digitonin did not significantly increase luciferase activity for TNF $\alpha$ , which is secreted via the fusion of post-Golgi transport carriers with the PM [51], indicating that TNF $\alpha$  is not encapsulated within extracellular vesicles (Figure 2E). Similar results were obtained for FGF2 and IL1 $\beta$ , suggesting that these UcPS cargo proteins, like TNF $\alpha$ , are released into the extracellular space in their free forms (Figure 2E). Consistent with previous reports [45–47, 58, 59], a significant fraction of Tau,  $\alpha$ SNC, SOD1 and Gal3 (11%, 14%, 22% and 23%, respectively) was secreted within vesicular structures, in addition to the main pool released in free form, as evidenced by the increase in luciferase activity upon addition of digitonin to the medium (Figure 2E). Importantly, digitonin by itself does not promote HiBit and LgBit interaction, especially for aggregation-prone proteins (Figure S2A). Additionally, inhibition of sphingomyelin phosphodiesterase 2 (N-SMase), a key enzyme involved in exosome biogenesis [60], using GW4869, decreased the secretion of Tau,  $\alpha$ SNC, SOD1 and Gal3 within vesicular structures, without significant effect on the secretion of TNF $\alpha$ , FGF2 and IL1 $\beta$  (Figure S2B). These findings further validate the ability of our assay to distinguish between free proteins and those encapsulated in extracellular vesicles. They also highlight that the majority of the UcPS cargoes investigated in our study are released as free, unencapsulated proteins.

Altogether, these results demonstrate that the engineered cell lines expressing distinct HiBit- and SBP-fused cargo proteins enabled us to establish a quantitative, versatile and sensitive cell-based assay to monitor protein secretion through both conventional and unconventional pathways, providing a reliable and straightforward method to study these processes.

## 2.2 | A Trapping Strategy Using the RUSH System to Identify Intermediate Compartments in UcPS

We next explored whether the split luciferase assay, in combination with the RUSH system, could be used to identify the intracellular compartments involved in UcPS. The RUSH system

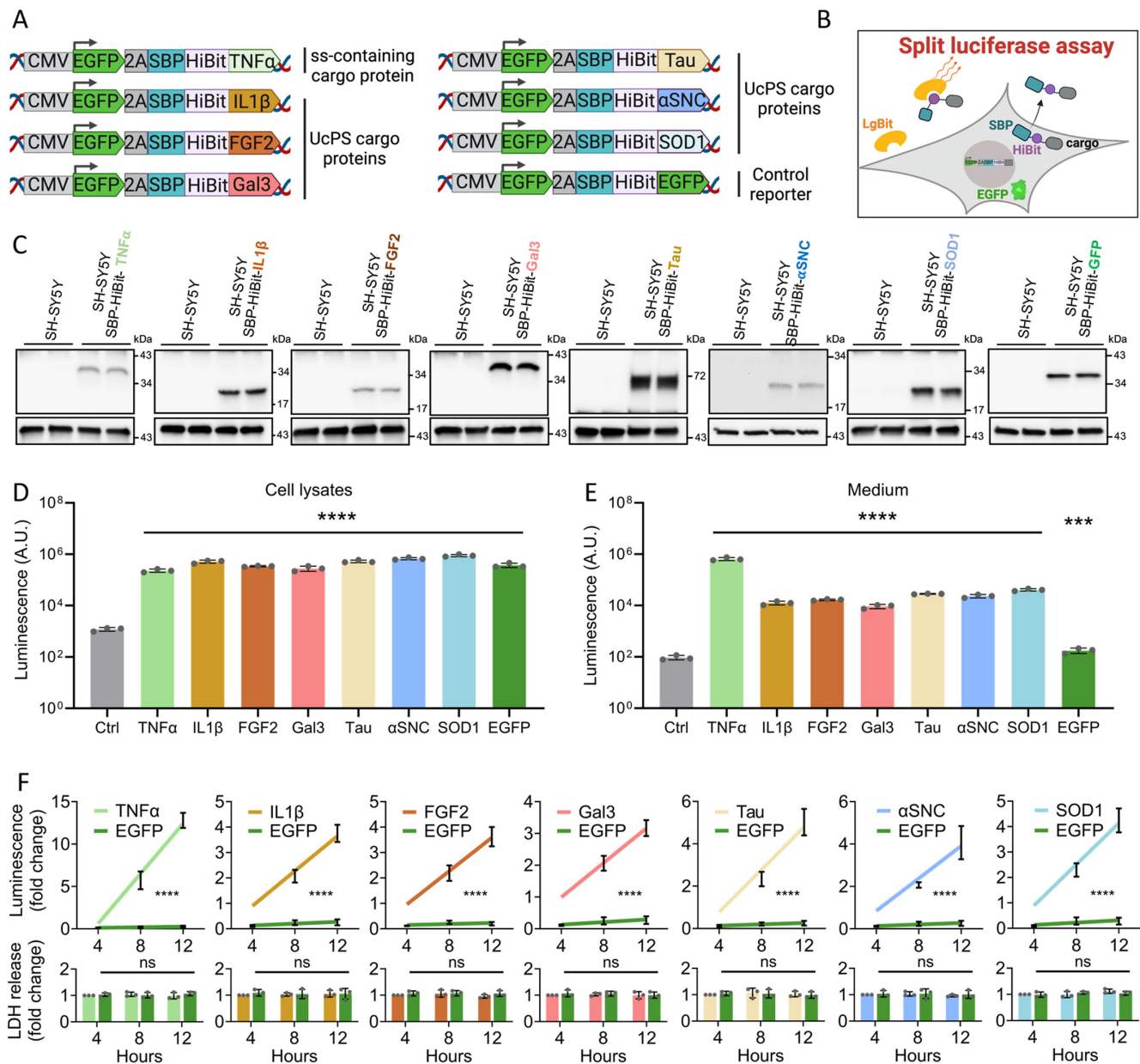


**FIGURE 1** | Sensitive and versatile cell-based assay for protein secretion. (A) Schematic representation of the plasmids used to generate the SH-SY5Y cell lines expressing different cargo proteins fused to the HiBit sequence and Strep tag. For all cell lines, the GFP tag, co-translationally self-cleaved with the 2A peptide, allowed selection of transduced cells by FACS (see Section 3). Although not depicted in the schematic, the sequence encoding the signal sequence (ss) of TNF $\alpha$  has been inserted upstream of the sequence encoding SBP in the corresponding construct. Regarding the IL1 $\beta$  construct, it encodes the mature form of the protein, the secreted form, which is generated following proteolytic cleavage by caspase 1. (B) Schematic representation of the split luciferase assay. (C) Stable cell lines expressing cargo proteins, either TNF $\alpha$ , IL1 $\beta$ , FGF2, Gal3, Tau,  $\alpha$ SNC, SOD1 and GFP fused to the HiBit sequence and Strep tag, were lysed, and the corresponding extracts subjected to SDS-PAGE, followed by Western blotting with anti-HiBit and anti- $\beta$ -actin antibodies. Non-transduced SH-SY5Y cells were used as a negative control. Samples were loaded on each gel in duplicate. (D and E) Quantification of cargo protein amount by split luciferase complementation assay from cell lysate (D) and medium (E) in non-transduced cells (Ctrl) and cells expressing the different reporters after incubation in complete medium for 12 h. The sensitivity of the assay is confirmed by a signal-to-noise ratio above 2-log (mean of  $n = 3 \pm SD$ ; \*\*\* $p < 0.001$ , \*\*\*\* $p < 0.0001$  vs. non-transduced cells [Ctrl] analyzed by one-way ANOVA followed by Dunnett's multiple comparison test). (F) Split luciferase complementation assay in SH-SY5Y cells expressing the different cargo proteins incubated in complete medium in a 12-h time course at 4-h intervals. The ratio of medium to lysate luminescence was quantified, and the values for each condition were normalized to  $t = 4$  h. As a control, split luciferase complementation assay was performed in SH-SY5Y cells expressing GFP fused to the HiBit sequence and Strep tag (mean of  $n = 3 \pm SD$ ; \*\*\*\* $p < 0.0001$  vs. EGFP luminescence when comparing slopes from linear regression model). LDH release was also monitored from each medium fraction (mean of  $n = 3 \pm SD$ ) and analyzed by two-way ANOVA followed by Dunnett's multiple comparison test. The specificity of the assay was validated by the luciferase activity, which increased over time for each cargo protein except for GFP, and by the absence of a difference in LDH release between all conditions.



relies on a “hook” consisting of a resident protein of a specific organelle fused to Strep, and a “reporter,” the cargo protein of interest fused with SBP [51]. Upon co-expression, the reporter binds to the hook via the Strep–SBP interaction (Figure 3A). This interaction can be disrupted by the addition of biotin, which competes for Strep with high affinity [51]. To implement this method, SH-SY5Y cells stably expressing TNF $\alpha$ , Tau,  $\alpha$ SNC, Gal3, IL1 $\beta$ , or FGF2 (each fused to the HiBit sequence and SBP) were transduced with a lentivirus to express a hook consisting of Strep fused N-terminally to a signal sequence and C-terminally to the KDEL motif, leading to Strep-KDEL hook localization within the ER lumen (Figure 3A). As expected, without biotin, this setup trapped TNF $\alpha$ , a signal sequence-containing cargo protein, preventing its secretion. Upon the addition of biotin, which disrupts the Strep–SBP interaction, TNF $\alpha$  secretion was

restored (Figure 3B). Conversely, when cells were transduced to express Strep fused with the invariant chain (Ii) at the N-terminal, resulting in a hook localized at the ER but with Strep oriented towards the cytosol [51], TNF $\alpha$  secretion was unaffected, with or without biotin (Figure 3B).

We next applied these trapping strategies to SH-SY5Y cells expressing UcPS cargo proteins (FGF2, Tau,  $\alpha$ SNC and Gal3) that lack a signal sequence for ER entry. Expression of the Strep-KDEL hook with Strep oriented within the ER lumen did not impact the secretion of either FGF2, Tau,  $\alpha$ SNC, or Gal3, regardless of the presence or absence of biotin (Figure 3C–F). However, when the hook was localized in the ER with Strep facing the cytosol (Ii-Strep), secretion of both FGF2, Tau,  $\alpha$ SNC and Gal3 was inhibited. This inhibition was reversed by biotin,

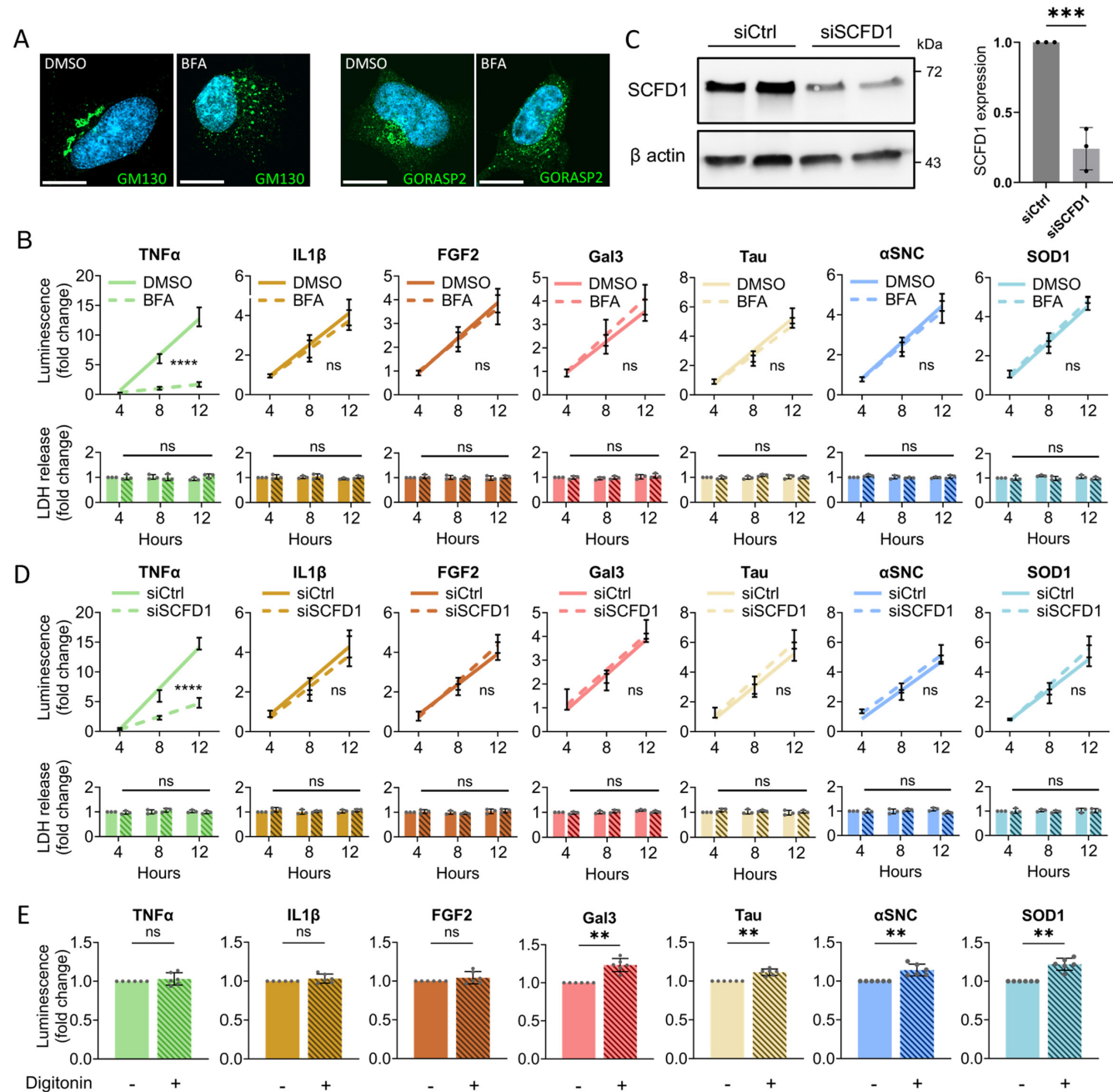


**FIGURE 2** | Legend on next page.

**FIGURE 2** | UcPS cargo proteins are secreted independently of the ER-Golgi secretory pathway and are differentially released in extracellular vesicles. (A) Representative confocal images showing immunofluorescence staining of Golgi membrane (GM130 and GORASP55 in green) and nuclei stained with DAPI (blue) from SH-SY5Y cells incubated in DMSO or 500 ng/mL BFA for 12 h. Scale bar: 10  $\mu$ m. (B) Split luciferase complementation assay in stable SH-SY5Y cells expressing HiBit-tagged cargo proteins, incubated in complete medium in the presence of DMSO or 500 ng/mL BFA for 12 h at 4-h intervals. The ratio of medium to lysate luminescence was quantified, and the values for each condition were normalized to the control sample (DMSO) at  $t = 4$  h (mean of  $n = 3 \pm \text{SD}$ ; \*\*\*\* $p < 0.0001$  vs. DMSO condition when comparing slopes from linear regression model). Bars in the bottom graphs indicate LDH release from each medium fraction (mean of  $n = 3 \pm \text{SD}$ ) analyzed by two-way ANOVA followed by Dunnett's multiple comparison test. (C) Left panel. SH-SY5Y cells were transfected with ctrl siRNA or siRNA targeting SCFD1. Three days after transfection, the knockdown efficiency of SCFD1 was assessed by Western blotting of total cell lysates with an anti-SCFD1 antibody.  $\beta$ -actin was used as a loading control. Samples from two independent experiments were loaded on the same gel. Right panel. Quantification of the knockdown efficiency of SCFD1 (mean of  $n = 3 \pm \text{SD}$ ; \*\*\* $p < 0.001$  vs. siCtrl condition) analyzed by Student's  $t$ -test. (D) Split luciferase complementation assay in stable SH-SY5Y cells expressing HiBit-tagged cargo proteins, transfected with ctrl siRNA and siRNA targeting SCFD1. Cells were incubated in complete medium for 12 h at 4-h intervals. The ratio of medium to lysate luminescence was quantified, and the values for each condition were normalized to the control sample (ctrl siRNA) at  $t = 4$  h (mean of  $n = 3 \pm \text{SD}$ ; \*\*\*\* $p < 0.0001$  vs. siCtrl condition, 1 when comparing slopes from linear regression model). Bars in the bottom graphs indicate LDH release from each medium fraction (mean of  $n = 3 \pm \text{SD}$ ) analyzed by two-way ANOVA followed by Dunnett's multiple comparison test. (E) Split luciferase complementation assay in medium collected after 12 h from SH-SY5Y cells expressing HiBit-tagged cargo proteins. For each cell line, collected medium was incubated in the presence or absence of 30  $\mu$ g/mL digitonin for 15 min on ice before luminescence quantification. For each experiment, values were normalized to medium samples incubated without digitonin (mean of  $n = 6 \pm \text{SD}$ ; \* $p \leq 0.05$ , \*\* $p \leq 0.01$  vs. (–) digitonin, analyzed by Kolmogorov–Smirnov's test).

confirming that their UcPS does not involve transport through the ER–ERGIC–Golgi axis (Figure 3C–F).

We extended this analysis to IL1 $\beta$ , another UcPS cargo protein that lacks a signal sequence for ER entry. Similar to FGF2, Tau,  $\alpha$ SNC and Gal3, IL1 $\beta$  secretion was blocked by the cytosol-oriented Ii-Strep hook, with secretion restored upon biotin addition (Figure 3G). However, the Strep-KDEL hook, which blocked TNF $\alpha$  secretion, also partially inhibited IL1 $\beta$  secretion (Figure 3G). These results suggest that a fraction of IL1 $\beta$  may transit through compartments associated with the conventional secretory pathway. This is consistent with recent studies indicating that IL1 $\beta$  secretion is mediated by the TMED10-channelled UcPS (THU) pathway, which relies on TMED10 oligomerization to form a channel that facilitates UcPS cargo translocation into the ERGIC [56, 57, 61]. Although the Strep-KDEL hook mainly localizes within the ER lumen [51], a small fraction may escape to the ERGIC and Golgi membrane before being retrieved back to the ER [62, 63]. This could explain its inhibitory effect on IL1 $\beta$  secretion, assuming IL1 $\beta$  is exclusively translocated into the ERGIC during THU-mediated UcPS [56, 57, 61].

Overall, our findings demonstrate that combining the NanoLuc Binary Technology with the RUSH system allows for the identification of intermediate compartments involved in UcPS, as evidenced by our results for IL1 $\beta$ , which was previously identified to traffic through the ERGIC for its release [56]. This highlights the potential of this method to reveal key steps and vesicular intermediates in UcPS pathways.

### 2.3 | Impact of SOD1 and Tau Mutations Linked to Familial Amyotrophic Lateral Sclerosis (ALS) and Tauopathies on Their UcPS

SOD1 and Tau proteins have garnered significant attention as pathological aggregation-prone proteins that accumulate in neurodegenerative diseases like ALS and tauopathies, such as Alzheimer's disease and frontotemporal dementia. Evidence

shows that SOD1 and Tau can spread from cell to cell after their release via UcPS [47, 58]. Under proteotoxic stress, often associated with lysosomal degradative dysfunction [9, 29], UcPS of these proteins may serve as an alternative pathway for clearing toxic materials, thereby preventing excessive cellular stress [37, 38, 58]. However, this process may also have the potential to cause propagation of toxic materials between cells, favoring disease progression at the organism level [29, 48]. We investigated whether disease-associated SOD1 and Tau mutations affect the UcPS-mediated intercellular spreading of these proteins using our cell-based assay. We first generated five SH-SY5Y cell lines expressing wild-type (wt) SOD1 and four SOD1 variants associated with familial ALS: G93A, D90A, A4V and D76Y, each fused to the HiBit sequence and Strep (Figure 4A). These mutations vary in their impact on SOD1 folding, function, aggregation and disease severity. The G93A, D90A and A4V mutations disrupt SOD1 folding and impair structural stability [64]. Notably, the A4V mutation, one of the most aggressive mutations, severely reduces SOD1 stability and enzymatic activity, leading to increased aggregation propensity and rapid disease progression. The G93A mutation induces a toxic gain of function, causing SOD1 misfolding and aggregation and is associated with severe neurodegeneration. In contrast, the D90A variant retains most of SOD1's enzymatic activity, though this varies among patients, leading to a milder clinical course. The D76Y mutation reduces the net repulsive charge of SOD1, affecting SOD1's electrostatic repulsion toward other molecular components. This mutation can also affect SOD1 stability and is associated with very slow disease progression [64]. Whether SOD1 mutations affect its secretion through UcPS remains to be elucidated. Western blot analysis of total cell lysates confirmed the expression of all SOD1 variants, although mutant forms exhibited lower expression levels compared to the wt, the most important reductions being observed for SOD1-G93A and SOD1-A4V (Figure 4B). To evaluate the secretion of these variants, cells were cultured in complete medium for 12 h, and their release was measured using our split luciferase complementation assays. No difference was detected between the secretion of wt-SOD1 and

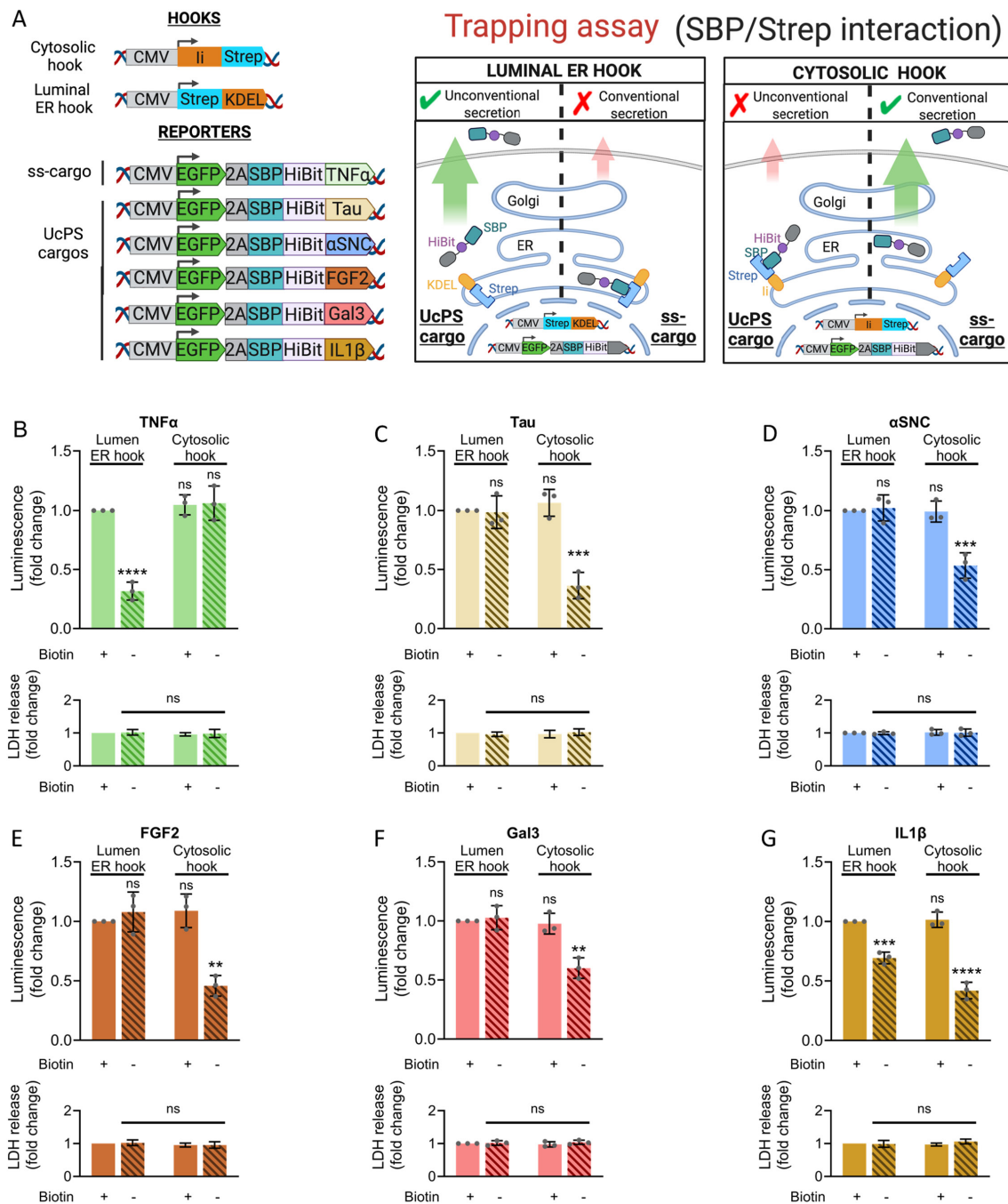


**FIGURE 3** | The RUSH system revealed the role of conventional secretory pathway compartments in IL1β UcPS. (A) Left panel, schematic representation of the plasmids used for the RUSH system. Hooks include Strep-KDEL, with Strep facing the ER lumen and Ii-Strep, also localized to the ER, but with Strep facing the cytosol. Reporters include TNFα, a cargo protein containing a signal sequence (ss) and five UcPS cargo proteins, including Tau, αSNC, FGF2, Gal3 and IL1β, all fused to the HiBit sequence and SBP tag. Right panel, Schematic representation of the different configurations used for the RUSH system. In SH-SY5Y cells, expression of an ER hook with Strep facing the cytosol is expected to inhibit secretion of UcPS cargo protein and have no effect on secretion of cargo protein containing a signal sequence (ss) that is transported along the ER-Golgi secretory pathway. In contrast, the expression of an ER hook with Strep facing the ER lumen is expected to have no effect on the secretion of UcPS cargo protein, but to prevent the secretion of ss-containing cargo protein. Importantly, the inhibition of cargo protein secretion by the Strep-SBP interaction is prevented by the addition of biotin. (B–G) Split luciferase complementation assay in SH-SY5Y cells expressing an ER hook facing either the ER lumen or the cytosol, and cargo proteins fused to the HiBit sequence and Strep tag including TNFα (B), Tau (C), αSNC (D), FGF2 (E), Gal3 (F) and IL1β (G). Cells were incubated for 12 h in complete medium in the presence or absence of 30 μM biotin. The ratio of medium to lysate luminescence was quantified and the values for each condition were normalized to the control sample (cells expressing a luminal ER hook with biotin) (mean of  $n = 3 \pm \text{SD}$ ;  $**p \leq 0.01$ ,  $***p \leq 0.001$ ,  $****p < 0.0001$  vs. lumen ER hook expression condition (+) Biotin, analyzed by two-way ANOVA followed by Tukey's multiple comparison test). Bars in the bottom graphs indicate LDH release from each medium fraction (mean of  $n = 3 \pm \text{SD}$ ) analyzed by two-way ANOVA followed by Tukey's multiple comparison test.



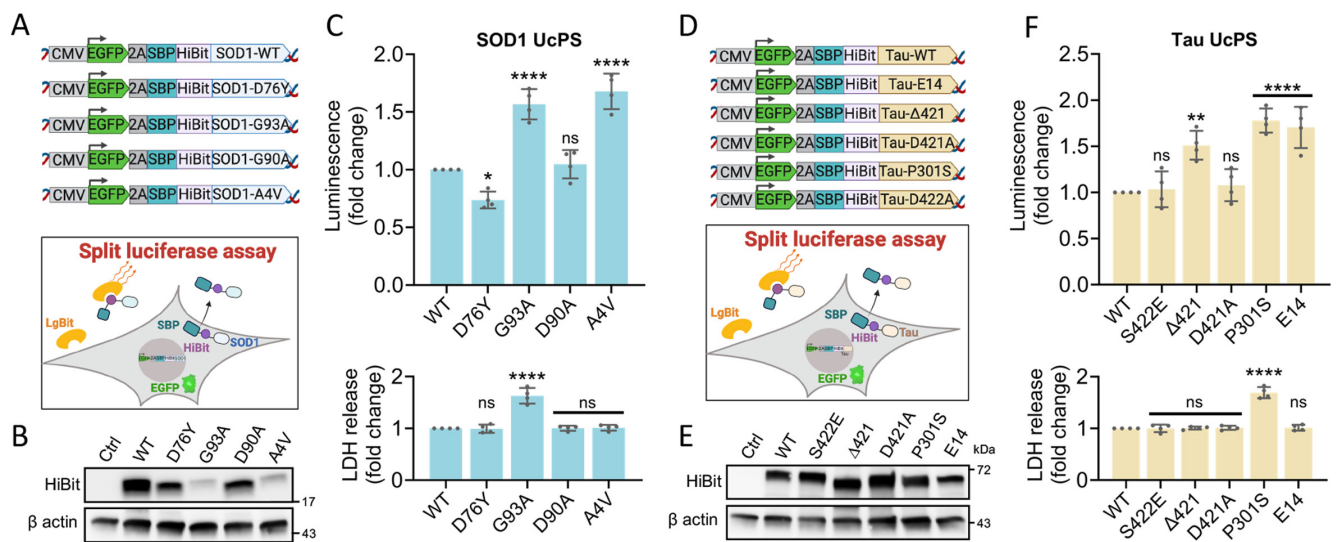


**FIGURE 4** | UCPs of SOD1 and Tau mutants/variants. (A) Top panel, schematic representation of the plasmids used to generate the SH-SY5Y cell lines expressing different SOD1 variants fused to the HiBit sequence and Strep tag. The SOD1 variants included SOD1-wt, SOD1-G93A, SOD1-D90A, SOD1-A4V and SOD1-D76Y. Bottom panel, schematic representation of the split luciferase assay. (B) Stable cell lines expressing the different SOD1 variants fused to the HiBit sequence and Strep tag were lysed and subjected to SDS-PAGE, followed by Western blotting with anti-HiBit and anti- $\beta$ -actin antibodies. Non-transduced SH-SY5Y cells were used as a negative control. (C) Split luciferase complementation assay in SH-SY5Y cells expressing SOD1 variants fused to the HiBit sequence and Strep tag, incubated in complete medium for 12 h. The ratio of medium to lysate luminescence was quantified, and the values for each condition were normalized to the control sample (cells expressing SOD1-wt) (mean of  $n = 4 \pm \text{SD}$ ;  $**p < 0.01$ ,  $***p < 0.001$ ,  $****p < 0.0001$  vs. SOD1-wt analyzed by one-way ANOVA followed by Dunnett's multiple comparison). Bars in the bottom graphs indicate LDH release from each medium fraction (mean of  $n = 4 \pm \text{SD}$ )  $****p \leq 0.0001$  analyzed by one-way ANOVA followed by Dunnett's multiple comparison test). (D) Top panel, schematic representation of the plasmids used to generate the SH-SY5Y cell lines expressing different Tau variants fused to the HiBit sequence and Strep tag. Tau variants included Tau-wt, Tau-S422E, Tau- $\Delta 421$ , Tau-D421A, Tau-P301S and Tau-E14. Bottom panel, schematic representation of the split luciferase assay. (E) Stable cell lines expressing the different Tau variants fused to the HiBit sequence and Strep tag were lysed and subjected to SDS-PAGE, followed by Western blotting with anti-HiBit and anti- $\beta$ -actin antibodies. Non-transduced SH-SY5Y cells were used as a negative control. (F) Split luciferase complementation assay in SH-SY5Y cells expressing Tau variants fused to the HiBit sequence and Strep tag incubated in complete medium for 12 h. The ratio of medium to lysate luminescence was quantified, and the values for each condition were normalized to the control sample (cells expressing Tau-wt) (mean of  $n = 4 \pm \text{SD}$ ;  $****p < 0.0001$  vs. Tau-wt analyzed by one-way ANOVA followed by Dunnett's multiple comparison test). Bars in the bottom graphs indicate LDH release from each medium fraction (mean of  $n = 4 \pm \text{SD}$ ) analyzed by one-way ANOVA followed by Dunnett's multiple comparison test.

D90A SOD1. However, the D76Y mutation decreased SOD1 secretion, whereas the G93A and A4V mutations promoted SOD1 secretion (Figure 4C, top panel and Figure S3A). Importantly, while LDH assays revealed no changes in cytosolic leakage for most of the SOD1 variants, confirming that the observed differences are due to altered secretion, the G93A mutation clearly increased cellular stress, as evidenced by the higher activity of LDH detected in the medium of the corresponding cells (Figure 4C, bottom panel), and the increase in the % of apoptotic cells (Figure S3B). The increased release of the G93A SOD1 variant is therefore likely the result of cell lysis/apoptosis as previously reported [65, 66]. These findings indicate that the D76Y and A4V SOD1 mutations not only influence protein stability, activity and aggregation but also significantly affect its secretion via UCPs. Interestingly, as observed for wt-SOD1, a significant fraction of the SOD1 mutants is secreted within vesicular structures (Figure S3C).

We next generated SH-SY5Y cell lines expressing several Tau variants, each fused to the Strep tag and HiBit sequence. These variants included S422E,  $\Delta 421$ , D421A, P301S and a Tau variant in which 14 serine/threonine residues were substituted with glutamate (E14), to mimic phosphorylation on

these residues [48, 67] (Figure 4D). Indeed, Tau undergoes various post-translational modifications, including extensive phosphorylation on multiple residues, which critically modulates its function and interaction with microtubules [68, 69]. Notably, aggregated hyperphosphorylated Tau is the main component of the neurofibrillary tangles observed in the brain of Alzheimer's disease patients [70], and several studies suggest that phosphorylation promotes Tau secretion [48, 71], with specific phosphorylated forms preferentially detected in the cerebrospinal fluid of Alzheimer's disease patients [72]. The P301S mutation, associated with familial frontotemporal dementia [73], accelerates Tau aggregation [74]. Similarly, the  $\Delta 421$  mutation, which results in C-terminus truncation, is found in neurofibrillary tangles [75] and enhances Tau aggregation property [76]. The D421A mutation prevents caspase-mediated cleavage at this site, preserving Tau's full-length form, while the S422E mutation mimics phosphorylation at serine 422, a modification linked to the inhibition of Tau cleavage at D421 and commonly found in aggregated Tau [77]. Western blot analysis of total cell lysates showed relatively homogeneous expression levels of all Tau variants (Figure 4E). As with the ALS-linked mutant SOD1, we cultured Tau-expressing cell lines in complete medium



for 12h and assessed Tau secretion using the split luciferase complementation assay. The D421A and S422E mutations had no significant effect on Tau secretion, whereas the  $\Delta$ 421 and E14 variants promoted Tau UcPS (Figure 4F, top panel and Figure S4A). Importantly, no differences in LDH release were observed across the different cell lines, ruling out cell lysis as a confounding factor in Tau secretion variability (Figure 4F, bottom panel). However, the increased secretion of P301S Tau was accompanied by an increase in LDH activity in the culture medium (Figure 4F, bottom panel), and an increase in the % of apoptotic cells (Figure S4B), suggesting that this variant undergoes non-specific release through cytosolic leakage. As observed for the SOD1 variants, a significant fraction of the Tau mutants is secreted within vesicular structures (Figure S4C).

Taken together, these results demonstrate that our assay allows the comparative analysis of different mutant forms of a given cargo protein. They also suggest that mutations in SOD1 and Tau can significantly affect their secretion via UcPS, potentially contributing to the pathogenesis of ALS and tauopathies.

## 2.4 | Targeted Screening of Alzheimer's Disease Risk Genes Reveals Key Factors in Tau UcPS

The intercellular propagation of Tau in Alzheimer's disease highlights the crucial need to identify molecular factors that regulate Tau UcPS and their role in neurodegenerative disease progression. A promising avenue for increasing our understanding of Alzheimer's disease is to investigate whether risk genes associated with the disease influence Tau UcPS. To explore this issue and further validate the robustness of our cell-based split luciferase complementation assay, we conducted a targeted screen of Alzheimer's disease risk genes to assess their role in Tau secretion through UcPS. We designed 96-well plates pre-arrayed with a selection of specific smart pool siRNAs targeting 46 distinct Alzheimer's risk genes [78]. These genes represent key players in cellular processes associated with neurodegeneration, including amyloid precursor protein (APP) processing, membrane trafficking and protein degradation [78–88]. Gene knockdowns were performed in SH-SY5Y cells expressing wt-Tau fused to the HiBit sequence and Strep tag. Three days after siRNA transfection, cells were washed and incubated for 12h in complete medium, and both cell lysates and medium were then harvested for the split luciferase complementation assay (Figure 5A). Our screen revealed that the knockdown of several genes modulated Tau UcPS. For example, genes such as angiotensin I converting enzyme (ACE), ADAM metalloproteinase domain 10 (ADAM10) and charged multivesicular body protein 2B (CHMP2B) prevented Tau UcPS upon knockdown, while genes like Cas scaffold protein family member 4 (CASS4), WW domain-containing oxidoreductase (WWOX) and Gelsolin (GSN) promoted Tau UcPS upon knockdown (Figures 5B and S5A). Interestingly, the knockdown of APP and several genes involved in the endolysosomal pathway, where amyloid-beta (A $\beta$ ) production occurs [89], strongly reduced Tau UcPS. These included ATP-binding cassette subfamily A member 7 (ABCA7) [79], bridging integrator 1 (BIN1) [80], phosphatidylinositol binding clathrin assembly protein (PICALM) [90] and sortilin-related receptor 1 (SORL1) [91], among others. In contrast, the

depletion of valosin-containing protein (VCP) [88], recently identified as a key factor in ribosome-associated quality control and important for APP expression, strongly promoted Tau UcPS (Figures 5B and S5A). Surprisingly, we also observed opposing effects on Tau UcPS following PSEN1 and PSEN2 knockdown. PSEN1 depletion reduced Tau UcPS, whereas depletion of PSEN2 promoted Tau UcPS (Figures 5B and S5A). PSEN1 and PSEN2 are homologous proteins, sharing approximately 67% amino acid sequence similarity, and both are components of the active  $\gamma$ -secretase complex involved in A $\beta$  generation. These apparently contradictory results may reflect a critical dynamic interplay between PSEN1 and PSEN2 influencing the activity of  $\gamma$ -secretase complex, as recently proposed [87]. Further investigation is needed to understand how these factors directly or indirectly impact Tau UcPS. However, importantly, when the same screen was performed in SH-SY5Y cells expressing Gal3 fused to the HiBit sequence and Strep tag, no significant changes in Gal3 UcPS were observed upon knockdown of these genes (Figures 5B and S5B). These findings suggest that the amyloidogenic processing of APP, a critical event in Alzheimer's pathology leading to A $\beta$  generation [92] and/or the associated endolysosomal stress [93, 94] may play a critical role in regulating Tau UcPS and, more broadly, contribute to Tau propagation and disease progression in Alzheimer's disease.

## 2.5 | A $\beta$ Peptide Promotes Tau UcPS

APP is a transmembrane protein containing a signal sequence, which allows its transport to the PM via the conventional ER/Golgi secretory pathway. At the cell surface, APP undergoes proteolytic cleavage by the  $\alpha$ -secretase, generating a neurotrophic factor through the so-called non-amyloidogenic pathway [95]. Under pathological conditions such as Alzheimer's disease, APP can be internalized through endocytosis and trafficked via the endolysosomal pathway. Within this pathway, sequential cleavages by the  $\beta$ - and  $\gamma$ -secretases lead to the generation of A $\beta$  peptides. The secretion and aggregation of A $\beta$  peptides contribute to the formation of extracellular plaques, a hallmark of Alzheimer's disease [92, 95]. Given that several Alzheimer's disease risk factors, including BIN1, ABCA7, PSEN1 and VCP, are known to modulate A $\beta$  peptide production and also influence Tau UcPS (as shown in Figure 5B), we hypothesized that the amyloidogenic pathway and A $\beta$  generation within the endolysosomal pathway may promote Tau UcPS. To test this hypothesis, we incubated SH-SY5Y cells expressing wt-Tau fused to the Strep tag and HiBit sequence with 1  $\mu$ M recombinant, fluorescently labeled A $\beta$ -42 peptide. After 24h incubation, we confirmed that the recombinant A $\beta$ -42 peptide was internalized and localized within the endolysosomal pathway, as evidenced by its colocalization with LAMP1 (Figure 5C), consistent with previous reports [96, 97]. Under these conditions, the split luciferase complementation assay revealed that the presence of recombinant A $\beta$ -42 peptide significantly enhanced Tau UcPS compared to control cells incubated with a scrambled peptide (Figure 5D). Notably, A $\beta$ -42 peptide had no effect on Gal3 UcPS (Figure 5E). Furthermore, LDH assays showed no changes in cytosolic leakage, confirming the absence of non-specific cell damage in these experiments (Figure 5D,E, bottom panels). Altogether, these results strongly suggest that A $\beta$ -42 peptide may play a direct role in regulating Tau UcPS, establishing a

functional link between two critical processes in Alzheimer’s disease progression: Aβ production and Tau dissemination.

2.6 | Discussion

The diversity of UcPS pathways—whether involving direct translocation of cargo protein across the PM or their initial incorporation into intracellular compartments—along with the

wide array of secreted factors produced by various cell types in response to stress or cellular demand [4, 7, 12, 98], underscores the need for standardized assays with well-controlled experimental settings to decipher mechanisms underlying UcPS. Here, we developed a quantitative and versatile cell-based assay that accurately measures the secretion of multiple UcPS cargo proteins. A key issue in studies on UcPS is ensuring that signal detection from proteins released in the extracellular medium is not the result of cell death or PM permeabilization. While

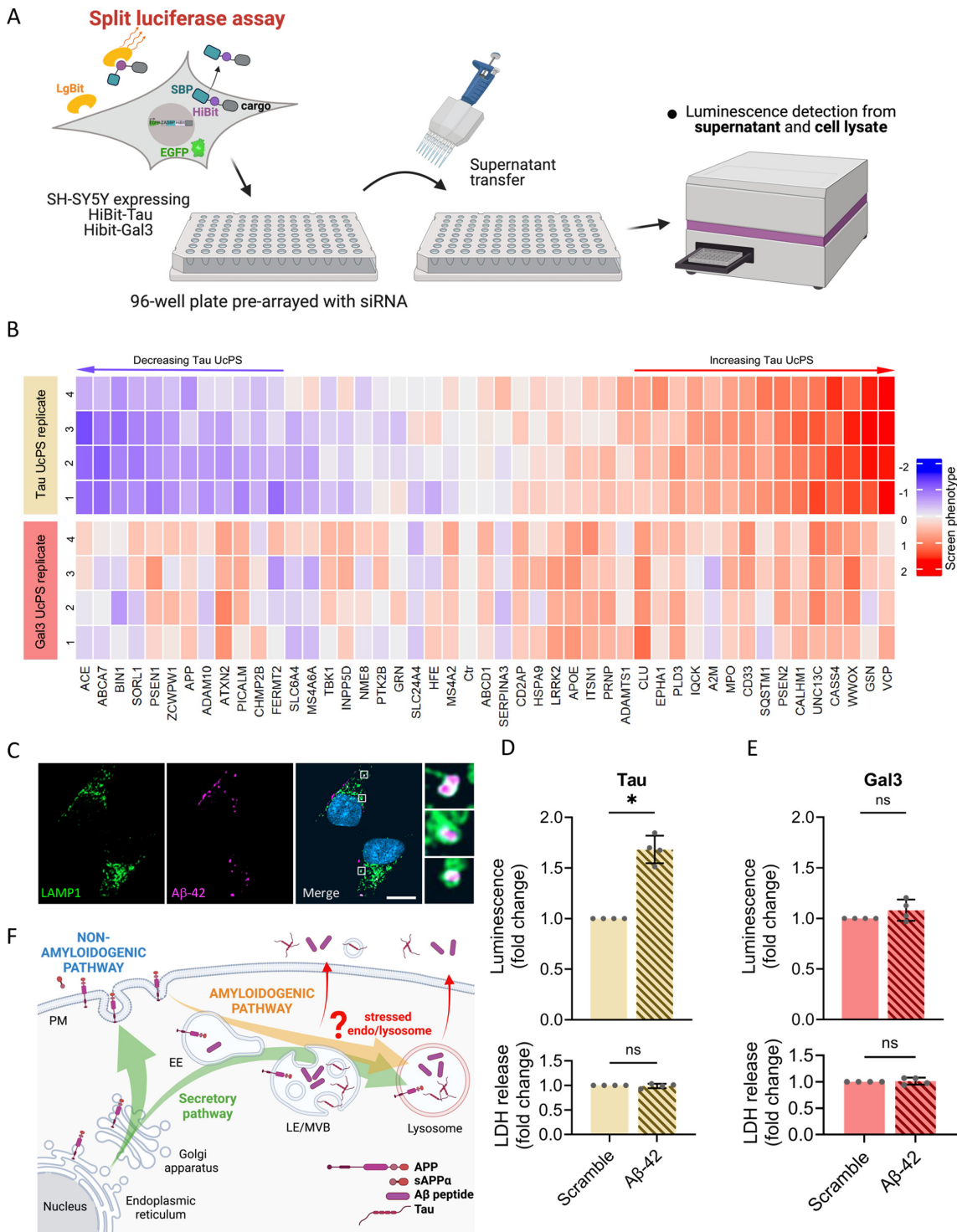


FIGURE 5 | Legend on next page.

**FIGURE 5** | Alzheimer's disease risk factors and A $\beta$  peptide influence Tau UcPS. (A) Schematic representation of the targeted screening workflow. SH-SY5Y cell lines expressing either Tau or Gal3 fused to the HiBit sequence and Strep tag were reverse-transfected in 96-well plates pre-arrayed with specific smart pool siRNA targeting Alzheimer's disease risk genes. After 24h, cells were forward-transfected and maintained in growth medium for another 2 days. Cells were then washed, incubated in complete medium, and after 12h, split luciferase complementation assay was performed on cell lysate and collected medium. (B) Heat map showing the results of the split luciferase complementation assay performed in SH-SY5Y cells expressing Tau and Gal3 fused to the HiBit sequence and Strep tag, transfected with siRNA targeting Alzheimer's disease risk genes, and incubated in complete medium for 12h. The ratio of medium to lysate luminescence was quantified, and the value in control sample (cells transfected with ctrl siRNA) was set as 1. Then, each value obtained with siRNA targeting Alzheimer's disease risk genes was calculated relative to control sample ( $n = 4$ ). The heat map shows the log2 value. Gene knockdowns that increase UcPS are noted in red, gene knockdowns that decrease UcPS are noted in blue. Detailed results are shown in Figure S5. (C) Representative confocal images of SH-SY5Y cells incubated in the absence or presence of 1  $\mu$ M fluorescent A $\beta$ -42 peptide for 24h. Immunofluorescence staining of endo/lysosomes with anti-LAMP1 antibody (green) shows that A $\beta$ -42 peptide (magenta) added to the culture medium is internalized and transported along the endocytic pathway. Nuclei are stained with DAPI (blue). Scale bar: 10  $\mu$ m. (D and E) Split luciferase complementation assay in stable SH-SY5Y cells expressing Tau (D) and Gal3 (E) fused to the HiBit sequence and Strep tag and incubated in complete medium for 24h in the presence or absence of 1  $\mu$ M A $\beta$ -42 peptide or 1  $\mu$ M scramble peptide. The ratio of medium to lysate luminescence was quantified, and the values for each condition were normalized to the control sample (cells incubated in the presence of scramble peptide) (mean of  $n = 5 \pm$  SD;  $*p \leq 0.05$  vs. scramble peptide (control condition) analyzed by Kolmogorov–Smirnov's test). Bars in the bottom graphs indicate LDH release from each medium fraction (mean of  $n = 5 \pm$  SD) analyzed by Kolmogorov–Smirnov's test. (F) Schematic illustrating the potential functional link between the amyloidogenic pathway generating A $\beta$  peptide and Tau UcPS, a critical event for Tau propagation during Alzheimer's disease pathogenesis. Since it has been reported that toxic misfolded Tau can be incorporated into endo/lysosomal compartments, which can then fuse with the PM and contribute to Tau UcPS, we hypothesize that A $\beta$  peptide, along the endocytic pathway, may induce stressed endo/lysosomes and convert these organelles into secretory compartments.

traditional controls such as LDH assays or the detection of intracellular markers like actin, tubulin, or GAPDH are useful, the ability to perform comparative and parallel analyses of different cargo proteins enhances the reliability and robustness of the data. By minimizing potential confounding effects from cell lysis or death across various experimental conditions, this approach can provide strong evidence for the specificity of distinct secretory pathways.

Overall, the split luciferase-based assay is highly customizable, allowing the analysis of multiple cargo proteins across various cell lines. Its sensitivity and adaptability to different assay formats make it an excellent tool for targeted genetic and pharmacological screening, as previously reported [99]. Furthermore, the assay can distinguish between free proteins and those encapsulated in extracellular vesicles, enhancing its versatility for studying UcPS. A key added value in our assay is the integration of the RUSH system. Originally designed to study protein trafficking through the ER–Golgi pathway [51], the RUSH system is also highly relevant for analyzing proteins lacking a signal sequence and for identifying intermediate compartments involved in UcPS. Consistent with previous findings [56], our RUSH-integrated assay provides evidence that a fraction of IL1 $\beta$  is released following its trafficking through compartments of the conventional secretory pathway. This aligns with the THU pathway, a seminal discovery in the field [56, 57, 100]. However, our results indicate that the THU pathway is not required for the secretion of other UcPS cargo proteins examined, such as FGF2, Tau,  $\alpha$ SNC and Gal3. For proteins secreted via Type III UcPS, the assay can be customized by targeting hook proteins to specific intracellular compartments. This flexibility allows the mapping of intermediate compartments through which cargo proteins traffic before secretion, providing valuable insights into the diverse pathways of UcPS.

An emerging area of research focuses on the role of UcPS in the progression of neurodegenerative diseases. The intracellular

accumulation of toxic, misfolded proteins like SOD1 and Tau is a hallmark of several neurodegenerative diseases. These misfolded proteins not only accumulate within cells in a cell-autonomous manner but also spread intercellularly along neuro-anatomical tracts [101, 102]. Evidence indicates that the release and transmission of aggregation-prone proteins, such as SOD1 in ALS and Tau in Alzheimer's disease and frontotemporal dementia, occurs via UcPS pathways [47, 48]. While most cases of these diseases are sporadic and arise from a combination of genetic, environmental and lifestyle factors, familial forms also exist, often driven by mutations in SOD1 and Tau [64, 78]. Our results indicate that mutations in the SOD1 and Tau genes not only affect protein folding and activity but also may contribute to ALS and tauopathy pathogenesis by altering their UcPS. For instance, the A4V SOD1 mutation, associated with rapidly progressive ALS [64], enhances SOD1 UcPS, whereas the D76Y mutation, linked to slower disease progression [64], reduces it. Interestingly, the D76Y mutation, which alters the net charge of SOD1 and its electrostatic interaction with other proteins, affects a diacidic motif previously identified as essential for SOD1 UcPS [22, 103]. While this motif could be viewed as indirectly influencing UcPS, it is highly conserved across SOD1 orthologs from yeast to mammals and also in the yeast acb1 protein, where it similarly regulates acb1 secretion via UcPS [22]. This conservation suggests that the D76 residue is part of a broader motif critical for exporting several UcPS cargo proteins. Given its role in modulating SOD1's net repulsive charge, it is likely that under conditions of proteotoxic stress and protein conformational changes, exposure of this motif facilitates cargo recognition and selection by recruiting specific binding partners. Our results also underscore the significance of post-translational modifications, such as phosphorylation, in regulating Tau UcPS [48, 71]. Together, these results suggest a subtle and complex interplay between the physicochemical properties of protein variants and their export via UcPS, with potential implications for disease progression and severity. A deeper understanding of these structure–UcPS–disease relationships is essential. Future research



should also explore whether different forms of the same UcPS cargo protein utilize distinct or overlapping secretory pathways and how these pathways may act synergistically during cellular stress. For instance, IL1 $\beta$  secretion occurs via both Types I and III UcPS pathways, depending on the intensity and duration of inflammatory stress [44, 104]. Similarly, cargo proteins associated with neurodegenerative diseases, such as Tau, SOD1 and  $\alpha$ SNC, have been proposed to follow distinct UcPS pathways for clearing toxic material when degradative processes are impaired [9, 17, 46, 105]. This is also illustrated by our results showing that SOD1 and Tau variants are secreted both as free proteins and within EVs (Figures S3C and S4C). The proposed underlying mechanisms include secretory autophagy, the misfolded-associated protein secretion (MAPS) pathway and/or the exocytosis of MVBs and lysosomes [47, 58]. In this context, our quantitative UcPS assay could serve as a powerful tool for identifying *cis*-regulatory motifs essential for cargo selection and recognition, as well as *trans*-effectors like chaperones that direct cargo proteins to specific or concurrent secretory routes under various stress conditions.

Finally, our assay for screening Alzheimer's disease risk factors has proven to be a powerful tool in identifying modifiers of Tau secretion and in establishing a functional link between A $\beta$  peptide generation and Tau UcPS. The progression of Alzheimer's disease involves two key sequential pathogenic processes. The first is the deposition of A $\beta$  peptide, which can occur during the early stages of the disease without necessarily being associated with neurodegeneration. The second involves Tau aggregation and spreading, typically linked to neuronal dysfunction and loss [106]. A major challenge in connecting these processes is their distinct subcellular localization and topological organization. APP is a transmembrane protein trafficked to the PM via the ER–Golgi secretory pathway, where it can be internalized and proteolytically cleaved within endolysosomal compartments to generate A $\beta$  peptide [92, 95]. In contrast, Tau is a cytosolic protein that primarily associates with microtubules but can be secreted via UcPS [48]. Interestingly, recent studies suggest that Tau and other aggregation-prone proteins can also be incorporated into endolysosomal compartments, which may be redirected for secretion under proteotoxic stress [37, 107–111]. Our data indicate that A $\beta$  peptides regulate Tau UcPS. This leads us to hypothesize that A $\beta$  peptide generation within endolysosomal compartments, along with the associated proteotoxic stress, alters their dynamics and function. Consequently, these compartments may be rerouted to the PM for exocytosis, releasing their contents, including Tau, into the extracellular space. It is likely that only a subset of these compartments is redirected for secretion, probably those in which the combined effects of A $\beta$  and Tau surpass a critical proteotoxic stress threshold. This would overwhelm the endolysosomal system's capacity to maintain its integrity and homeostasis [9], triggering Tau pathology and facilitating its spreading through endolysosomal-mediated UcPS (Figure 5F). In summary, the interplay between A $\beta$  peptide generation and Tau incorporation into the endolysosomal pathway may establish and perpetuate a pathological cycle, potentially accounting for the sequential progression of Alzheimer's disease. This model offers a valuable framework for further exploring the role of endo/lysosomes and UcPS in Alzheimer's disease pathogenesis [9, 93, 105]. However, it is important to recognize that this seemingly straightforward framework is likely more

complex, as mentioned earlier, with studies suggesting that Tau can also be secreted through Type I UcPS independently of the endo/lysosomal compartments [48, 49]. Understanding how distinct UcPS pathways can be mutually regulated, function synergistically, or be differentially impacted under cellular stress conditions is a critical area for future research.

In conclusion, the field of UcPS is rapidly evolving, with ongoing research aimed at uncovering its intricate mechanisms, its role in health and disease and its therapeutic potential. While the development of *in vivo* models that accurately recapitulate the molecular and cellular dynamics of UcPS remains a significant challenge, our versatile assay provides a robust platform to address fundamental questions in the field and advance our understanding of cellular communication.

### 3 | Materials and Methods

#### 3.1 | Antibodies, Reagents and Plasmids

Antibodies used in this study included: mouse monoclonal antibodies anti-HiBit (Promega, #CS2006A01), anti-GM130 (BD Biosciences, #610823), anti-GAPDH coupled to HRP (Cell Signaling Technology, #51332s), anti-actin coupled to HRP (Invitrogen, #MA5-11869), rabbit monoclonal antibody anti-LAMP1 (Cell Signaling Technology, #9091s), anti-GORASP2 (ProteinTech, #10598-1-AP), secondary antibodies donkey anti-sheep IgG-Alexa Fluor 594 (Invitrogen, #A11016), goat anti-mouse IgG-Alexa Fluor 488 (Invitrogen, #A11029), goat anti-mouse IgG-546 (Invitrogen, #A11030) and secondary antibody mouse IgG $\kappa$  conjugated to HRP (Jackson Immuno Research, #115-035-174).

Reagents used in this study were obtained from the following sources. Dulbecco's modified Eagle's medium (DMEM), Sigma, #D8437), Dulbecco's phosphate-buffered saline (D-PBS, Sigma, #D8537), MEM Non-essential amino acid solution (Sigma, #M7145), Penicillin/Streptomycin (Gibco, #15140-122), L-glutamine (Sigma, #G7513), fetal bovine serum (FBS; Gibco, #10270-106), Trypsin (Gibco, #25300-054), Puromycin (Sigma, #P9620), G-418 (Sigma, #4727878001), OptiMEM (Gibco, #31985-062), BFA (Sigma, #B6542), GW4869 (Sigma, #D1692), Biotin (Sigma, #B4639), Universal Mycoplasma Detection Kit (ATCC, #ATCC30-1012K), View plate 96F TC (Black, Clear bottom, PerkinElmer #6005182), Lipofectamine2000 transfection reagent (Invitrogen, #11668019), *TransIT*-2020 transfection reagent (Mirus, #MIR5400), Polybrene (Millipore Corp, #TR-1003-G), 0.45  $\mu$ m low protein binding membrane (VWR International, #28145-479), Protease inhibitor cocktail (Sigma, #11836170001), Dako fluorescent mounting medium (Agilent, #S3023), DAPI (4,6-diamidino-2-phenylindole; ThermoFisher, #P36935), Mini-protean TGX stain free gels 4%–20% (Bio-Rad, #4561094), TransBlot Turbo Midi-Size Nitrocellular membrane (Bio-Rad, #1704271), ECL Western Blotting Detection Reagent (Bio-Rad, #170-5061 and GeneTex, #GTX14698), Nano-Glo HiBit Extracellular Detection system (Promega, #N2421), Nano-Glo HiBit Lytic Detection system (Promega, #N3040), LDH Assay Kit (Abcam, #ab102526), Annexin V-FITC Apoptosis Staining/Detection Kit (abcam, #ab14085), Color prestained protein standard (Biolabs, #P7719S),  $\beta$ -amyloid (1–42) Hilyte



TM Fluor 555-labeled (Anaspec, #AS-60480-01),  $\beta$ -amyloid 1–42 (Anaspec, #AS-20276) and scramble- $\beta$ -amyloid 1–42 (Anaspec, #AS-25382).

Plasmids included pcDNA3.1-GFP-2A-HiBit-Tau, pcDNA3.1-GFP-2A-HiBit- $\alpha$ SNC, pcDNA3.1-GFP-2A-HiBit-Gal3, pcDNA3.1-GFP-2A-HiBit-PAUF, pcDNA3.1-GFP-2A-HiBit-IL1 $\beta$ , pcDNA3.1-GFP-2A-HiBit-FGF2, pcDNA3.1-GFP-2A-HiBit-SOD1, pcDNA3.1-GFP-2A-HiBit-EGFP, pcDNA3.1-GFP-2A-HiBit-SOD1-A4V, pcDNA3.1-GFP-2A-HiBit-SOD1-D76Y, pcDNA3.1-GFP-2A-HiBit-SOD1-G90A, pcDNA3.1-GFP-2A-HiBit-SOD1-G93A, pcDNA3.1-GFP-2A-HiBit-Tau-E14, pcDNA3.1-GFP-2A-HiBit-TauD421A, pcDNA3.1-GFP-2A-HiBit-Tau-P301S, pcDNA3.1-GFP-2A-HiBit-Tau-D422E and pcDNA3.1-GFP-2A-HiBit-Tau- $\Delta$ 421 (ThermoFisher scientific). pCDH-Str-KDEL-neomycin was a gift from Franck Perez (Addgene plasmid #65307; <http://n2t.net/addgene:65307>; RRID:Addgene\_65307) [51]. pCDH-Str-Ii was a gift from Franck Perez (Addgene plasmid # 65313; <http://n2t.net/addgene:65313>; RRID:Addgene\_65313) [51].

### 3.2 | Cell Culture

The neuroblastoma cell line SH-SY5Y (ATCC) was grown in complete culture medium consisting of DMEM (Sigma, #D8437) supplemented with 10% heat-inactivated FBS (Gibco, #10270-106), 100 U/mL penicillin, 100  $\mu$ g/mL streptomycin (Gibco, #15140-122) and 2 mM L-glutamine (Sigma, #G7513) and maintained in a humidified atmosphere containing 5% CO<sub>2</sub> at 37°C. The cells were tested every month using the Universal Mycoplasma Detection Kit (ATCC, #ATCC30-1012K) to confirm the absence of mycoplasma contamination. To generate SH-SY5Y cell lines stably expressing the different cargo proteins fused to the HiBit and SBP, SH-SY5Y cells were transfected with the corresponding plasmids using TransIT-2020 transfection reagent (Mirus, #MIR5400), according to the manufacturer's recommendations. After 2 days, transfected cells were selected with 600  $\mu$ g/mL G-418 (Sigma, #4727878001) for 1 week. GFP-positive cells were then isolated by fluorescence-activated cell sorting (FACS). After expansion into a six-well plate format, the cell lines were assessed by Western blot analysis.

### 3.3 | Split Luciferase Complementation Assay

SH-SY5Y cells expressing the HiBit tagged reporter were cultured in a 96-well plate 96F TC (Black, Clear bottom, PerkinElmer #6005182) and incubated in complete medium for the indicated time. The split luciferase complementation assay was performed from 100  $\mu$ L of cell culture medium using the Nano-Glo HiBit Extracellular Detection System Kit (#N2421, Promega) and from 100  $\mu$ L of cells permeabilized using the Nano-Glo HiBit Lytic Detection System Kit (#N3040, Promega) according to the manufacturer's instructions. This protocol is based on the established concept of bimolecular fluorescence complementation (BiFC), and detects reporter luciferase activity only after complementation in the presence of LgBiT. The luminescent signal was measured using a Tecan Microplate reader Infinite 500 at the Arpege pharmacological screening platform (Biocampus, UM-CNRS-INSERM, Montpellier, France). The

ratio of medium to lysate luminescence was quantified, and the values were normalized to the control sample for each condition. For split luciferase complementation assays performed from cytosolic fractions, cells were washed three times with PBS, harvested by scraping, centrifuged at 600g for 5 min, and homogenized by passing through a 22G needle in a 1.5 $\times$  cell pellet volume of B88 buffer (20 mM Hepes-KOH, pH 7.2, 250 mM sorbitol, 150 mM potassium acetate and 5 mM magnesium acetate) plus cocktail protease inhibitors (Sigma-Aldrich). The cell homogenates were first centrifuged at 1000g for 10 min to remove unbroken cells and nuclei and then at 100 000g for 1 h to collect total membranes. Supernatant solutions were collected and used as cytosolic fractions. A total of 100  $\mu$ L of cytosolic fractions was then incubated in the presence or absence of 30  $\mu$ g/mL digitonin and Nano-Glo HiBit Extracellular reagent.

### 3.4 | siRNA-Mediated Knockdown

For specific single siRNA transfection with Smart pools siRNA, SH-SY5Y cells were transfected using Lipofectamine 2000 transfection reagent (Invitrogen, #11668019) according to the manufacturer's recommendations. Smart pools siRNAs were purchased from Dharmacon. The siRNA sequences used were ON-TARGETplus non-targeting pool (#D-001810-10-50) 5'-UGGUUUACAUGUCGACUAA-3', 5'-UGGUUUA CAUGUUGUGUGA-3', 5'-UGGUUUACAUGUUUCUGA-3', 5'-UGGUUUACAUGUUUCCUA-3'. ON-TARGETplus human SCFD1 siRNA smartpool (#L-010943-01-0005) 5'-AAGCAUUGGU GCACGAUGU-3', 5'-GACAAGAAACUUCGAGAAA-3', 5'-GUG CCAGGAUCUUCGAAAU-3' and 5'-GAUAUCACAGACACG GAAA-3'. The cells were reverse-transfected with specific individual siRNAs (75 nM final concentration per well) in the culture medium without antibiotics. After 4–6 h, the transfection medium was replaced with normal culture medium. After 24 h, the cells were forward-transfected with 75 nM siRNA as before, and the cells were maintained in culture medium for two additional days. For the targeted screening of Alzheimer's disease risk genes, SH-SY5Y cells expressing either wt-Tau or Gal3 fused to the HiBit sequence and Strep tag were reverse transfected in 96-well plates pre-arrayed with specific smart pools siRNA (Dharmacon) targeting selected genes (Table S1). Briefly, 5000 SH-SY5Y cells suspended in 80  $\mu$ L of complete medium without antibiotics were seeded into 96-well plates containing 20  $\mu$ L of 250 nM siRNA and 0.5% (v/v) lipofectamine 2000 in OptiMEM (Gibco, #31985-062). After 4–6 h, the transfection medium was replaced with normal culture medium. After 24 h, the cells were forward-transfected and maintained in culture medium for two additional days.

### 3.5 | Cell Lysis/Apoptosis Analysis

LDH release was monitored from cell culture media collected at the indicated times to assess the extent of PM damage and cell death using a commercially available LDH Assay Kit (Abcam, #ab102526), according to the manufacturer's recommendations. Analysis of cell apoptosis was assessed by the translocation of phosphatidylserine (PS) from the inner to the outer leaflet of the PM monitored using annexin V FITC assays. Briefly, detached cells were washed with annexin binding buffer (10 mM HEPES, 150 mM NaCl, 5 mM KCl, 1 mM MgCl<sub>2</sub> and 1.8 mM CaCl<sub>2</sub>).

Supernatants were then removed, and 100  $\mu$ L annexin binding buffer with fluorescein isothiocyanate (FITC)-conjugated annexin-V (1  $\mu$ M) was added to each cell pellet. Cells were stained for 20 min at room temperature, and immediately before collection, 400  $\mu$ L of annexin binding buffer was added to each sample. Fluorescent signals were then collected on an LSR Fortessa (BD Biosciences).

### 3.6 | Lentivirus Production and Transduction

Lentivirus was produced by the vector core facility of Montpellier (Plateforme de Vectorologie de Montpellier, Biocampus, UM-CNRS-INSERM, Montpellier, France). Briefly, lentivirus was generated in HEK293T cells transfected using the calcium phosphate method. At 50% confluence, HEK293T cells grown in complete medium without penicillin/streptomycin were transiently transfected with a lentiviral vector, either pCDH-Str-KDEL (Addgene plasmid #65307) for Strep-KDEL protein expression with Strep directed to the ER lumen, or pCDH-Str-Ii (Addgene plasmid # 65313) for Strep-Ii protein expression with Strep directed to the cytosol, together with the HIV packaging plasmid psPAX2 and the plasmid pMD2G, which codes for the vesicular stomatitis virus envelope glycoprotein G. After transfection (24 h), the medium was refreshed, and after an additional 24 h, virus was collected and filtered through a 0.45  $\mu$ m low protein binding membrane (VWR International, #28145-479), and concentrated on sucrose by ultracentrifugation at 17 000 g for 1.5 h, at 4°C. A total of 15  $\mu$ L of virus was used to infect ~1 million target cells plated in a 10-cm dish to a final volume of 10 mL. Medium was supplemented with 8  $\mu$ g/mL polybrene (Millipore Corp, #TR-1003-G) without penicillin/streptomycin. After 24 h, the medium was replaced with fresh medium, and after an additional 24 h incubation period, 2  $\mu$ g/mL puromycin (Sigma, #P9620) was added to select transduced cells.

### 3.7 | Western Blotting

Cells were lysed for 30 min on ice in lysis buffer (50 mM Tris, pH 7.4, 150 mM NaCl, 0.1% SDS, 1% [v/v] Triton X-100 and 0.5% sodium deoxycholate) supplemented with a protease inhibitor cocktail (Sigma, #11836170001), 1 mM Na<sub>3</sub>VO<sub>4</sub> and 25 mM sodium fluoride, and centrifuged at 16 000 g for 15 min. Samples were incubated with 1× sodium dodecyl sulfate (SDS) sample buffer at 95°C for 10 min, resolved by SDS-PAGE using 4%–20% Mini-protean TGX stain-free gels (Bio-Rad, #4561094), and transferred to a nitrocellulose membrane (Bio-Rad, #1704271). Membranes were blocked with 5% (w/v) BSA in PBS containing 0.1% Tween 20 (PBS-T) for 30 min at room temperature, and incubated with appropriate primary antibodies overnight at 4°C in PBS-T containing 5% (w/v) BSA. The membranes were then washed 3 × 15 min in PBS-T and incubated with the appropriate HRP-conjugated secondary antibody for 1 h at room temperature in PBS-T containing 5% (w/v) BSA. The membranes were then washed again for 3 × 15 min in PBS-T, and immunoreactive bands were detected with an enhanced chemiluminescence method (ECL Western Blotting Detection Reagent (Bio-Rad, #170-5061 or GeneTex, #GTX14698)) and signal was acquired with a ChemiDoc MP Imaging System (Bio-Rad).

### 3.8 | Immunofluorescence Microscopy

The cells grown on coverslips were fixed with cold methanol for 10 min at –20°C or with 4% (w/v) PFA in PBS for 15 min at room temperature. Cells fixed with PFA were permeabilized with 0.1% Triton X-100 in PBS at room temperature and then incubated with blocking buffer (2.5% [v/v] FCS, 0.1% Triton X-100 in PBS) for 30 min at room temperature. The cells were then incubated with primary antibodies diluted in blocking buffer for 1 h at room temperature, followed by PBS wash and incubation with secondary antibodies. Secondary antibodies conjugated with Alexa Fluor 488 or 568 were diluted in blocking buffer and incubated for 1 h at room temperature. Samples were mounted using Dako fluorescent mounting medium (Agilent, # S3023) with DAPI (ThermoFisher, #P36935). Images were acquired using a Leica SP8 laser confocal laser scanning microscope with a 40× objective at the imaging facility MRI (Biocampus, UM-CNRS-INSERM, Montpellier, France). Images displayed in the figures are representative single Z-slices. After acquisition, images were processed using an Airyscan processing tool on the ZEN software provided by Zeiss.

### 3.9 | Statistical Analysis

The data represent the mean  $\pm$  standard deviation (SD). Statistics were performed using the GraphPad Prism 10 software. Statistical tests were performed as specified in the figure legends. Results of the statistical analyses are displayed in the figures. *p* values < 0.05 were considered statistically significant. \**p* < 0.05, \*\**p* < 0.01, \*\*\**p* < 0.001 and \*\*\*\**p* < 0.0001.

#### Author Contributions

**Morgane Denus:** investigation, validation, formal analysis, visualization. **Aurore Filaquier:** investigation, validation, formal analysis, visualization. **William Fargues:** investigation, validation, formal analysis, visualization. **Eloïse Néel:** investigation, validation, formal analysis, visualization. **Sarah E. Stewart:** conceptualization, methodology, writing – review and editing. **Maëlle Colladant:** investigation. **Thomas Curel:** investigation. **Alexandre Mezghrani:** conceptualization, methodology, writing – review and editing. **Philippe Marin:** conceptualization, methodology, writing – review and editing. **Sylvie Claeysen:** conceptualization, methodology, writing – review and editing. **David C. Rubinsztein:** conceptualization, methodology, writing – review and editing. **Marie-Laure Parmentier:** conceptualization, methodology, formal analysis, writing – original draft, writing – review and editing, visualization, supervision, project administration, funding acquisition. **Julien Villeneuve:** conceptualization, methodology, formal analysis, writing – original draft, writing – review and editing, visualization, supervision, project administration, funding acquisition. All authors approved the publication of this study.

#### Acknowledgments

Julien Villeneuve acknowledges support from the Centre National de la Recherche Scientifique (CNRS), the Institut National pour la Santé et la Recherche Médicale (INSERM), the Université de Montpellier, the Fondation Vaincre Alzheimer, the Association France Parkinson, the Association France Alzheimer et maladies apparentées, the Fédération pour la Recherche sur le Cerveau (FRC), the Fondation pour la Recherche Médicale (FRM) (MND202310017892) and the Agence

Nationale de la Recherche (ANR-23-CE16-0012) and (ANR-24-CE16-5161-02). Marie-Laure Parmentier acknowledges support from the Centre of Excellence in Neurodegeneration (CoEN) of Montpellier. Sarah E. Stewart acknowledges support from the Australian Research Council (DE200100611). David C. Rubinsztein's work is supported by the UK Dementia Research Institute (through UK DRI Ltd.), principally funded by the UK Medical Research Council and the National Institute for Health Research Cambridge Biomedical Research Centre at Addenbrooke's Hospital. The views expressed are those of the author(s) and not necessarily those of the NHS, the NIHR, or the Department of Health and Social Care. Split luciferase complementation assays were performed using the facilities of the Arpege pharmacological screening platform, viral productions were performed using the vector core facility of Montpellier (Plateforme de Vectorologie de Montpellier, PVM), and confocal microscopy analysis was performed using the imaging facility MRI, member of the national infrastructure France-BioImaging, supported by the French National Research Agency (ANR-10-INBS-04, "Investments for the Future") (Biocampus, UM-CNRS-INSERM, Montpellier, France).

## Ethics Statement

The authors have nothing to report.

## Conflicts of Interest

David C. Rubinsztein is a consultant for Drishti Discoveries, PAQ Therapeutics, MindRank AI, Retro Biosciences, Alexion Pharma International Operations Limited and Nido Biosciences. The other authors declare no conflicts of interest.

## Data Availability Statement

All data supporting the findings of the manuscript are included in Figures 1–5 and S1–S5. Raw data for the presented figures are available upon request.

## Peer Review

The peer review history for this article is available at <https://www.webofscience.com/api/gateway/wos/peer-review/10.1111/tra.70009>.

## References

1. A. Rubartelli, F. Cozzolino, M. Talio, and R. Sitia, "A Novel Secretory Pathway for Interleukin-1 Beta, a Protein Lacking a Signal Sequence," *EMBO Journal* 9, no. 5 (1990): 1503–1510.
2. A. Rubartelli, A. Bajetto, G. Allavena, E. Wollman, and R. Sitia, "Secretion of Thioredoxin by Normal and Neoplastic Cells Through a Leaderless Secretory Pathway," *Journal of Biological Chemistry* 267, no. 34 (1992): 24161–24164.
3. M. A. Kinseth, C. Anjard, D. Fuller, G. Guizzunti, W. F. Loomis, and V. Malhotra, "The Golgi-Associated Protein GRASP Is Required for Unconventional Protein Secretion During Development," *Cell* 130, no. 3 (2007): 524–534.
4. M. Zhang and R. Schekman, "Unconventional Secretion, Unconventional Solutions," *Science* 340 (2013): 559–561.
5. C. Rabouille, V. Malhotra, and W. Nickel, "Diversity in Unconventional Protein Secretion," *Journal of Cell Science* 125 (2012): 5251–5255.
6. E. Dimou and W. Nickel, "Unconventional Mechanisms of Eukaryotic Protein Secretion," *Current Biology* 28 (2018): R406–R410.
7. A. Filaquier, P. Marin, M. L. Parmentier, and J. Villeneuve, "Roads and Hubs of Unconventional Protein Secretion," *Current Opinion in Cell Biology* 75 (2022): 102072.
8. M. Chiritoiu-Butnaru, S. E. Stewart, M. Zhang, V. Malhotra, and J. Villeneuve, "Editorial: Unconventional Protein Secretion: From

Basic Mechanisms to Dysregulation in Disease," *Frontiers in Cell and Development Biology* 10 (2022): 1088002.

9. E. Néel, M. Chiritoiu-Butnaru, W. Fargues, et al., "The Endolysosomal System in Conventional and Unconventional Protein Secretion," *Journal of Cell Biology* 223, no. 9 (2024): e202404152.

10. M. Denus, W. Fargues, A. Filaquier, et al., "Unconventional Protein Secretion—New Perspectives in Protein Trafficking," *Medical Science* 40, no. 3 (2024): 267–274.

11. R. W. Schekman, "Retrospective: George E. Palade (1912–2008)," *Science* 322, no. 5902 (2008): 695.

12. C. Rabouille, "Pathways of Unconventional Protein Secretion," *Trends in Cell Biology* 27, no. 3 (2017): 230–240.

13. M. T. Pallotta and W. Nickel, "FGF2 and IL-1 $\beta$ —Explorers of Unconventional Secretory Pathways at a Glance," *Journal of Cell Science* 133, no. 21 (2020): jcs250449, <https://pubmed.ncbi.nlm.nih.gov/33154173/>.

14. M. Zhang, S. J. Kenny, L. Ge, K. Xu, and R. Schekman, "Translocation of Interleukin-1 $\beta$  Into a Vesicle Intermediate in Autophagy-Mediated Secretion," *eLife* 4 (2015): e11205.

15. J. Villeneuve, L. Bassaganyas, S. Lepreux, et al., "Unconventional Secretion of FABP4 by Endosomes and Secretory Lysosomes," *Journal of Cell Biology* 217, no. 2 (2018): 649–665.

16. N. Dupont, S. Jiang, M. Pilli, W. Ornatowski, D. Bhattacharya, and V. Deretic, "Autophagy-Based Unconventional Secretory Pathway for Extracellular Delivery of IL-1 $\beta$ ," *EMBO Journal* 30, no. 23 (2011): 4701–4711.

17. J. G. Lee, S. Takahama, G. Zhang, S. I. Tomarev, and Y. Ye, "Unconventional Secretion of Misfolded Proteins Promotes Adaptation to Proteasome Dysfunction in Mammalian Cells," *Nature Cell Biology* 18 (2016): 765–776.

18. D. A. Liu, K. Tao, B. Wu, et al., "A Phosphoinositide Switch Mediates Exocyst Recruitment to Multivesicular Endosomes for Exosome Secretion," *Nature Communications* 14, no. 1 (2023): 6883.

19. S. Buratta, B. Tancini, K. Sagini, et al., "Lysosomal Exocytosis, Exosome Release and Secretory Autophagy: The Autophagic- and Endo-Lysosomal Systems Go Extracellular," *International Journal of Molecular Sciences* 21, no. 7 (2020): 2576, <https://doi.org/10.3390/ijms21072576>.

20. C. Bruns, J. M. McCaffery, A. J. Curwin, J. M. Duran, and V. Malhotra, "Biogenesis of a Novel Compartment for Autophagosome-Mediated Unconventional Protein Secretion," *Journal of Cell Biology* 195, no. 6 (2011): 979–992.

21. A. J. Curwin, N. Brouwers, Y. Alonso, et al., "ESCRT-III Drives the Final Stages of CUPS Maturation for Unconventional Protein Secretion," *eLife* 5 (2016): e16299.

22. D. Cruz-Garcia, N. Brouwers, J. M. Duran, G. Mora, A. J. Curwin, and V. Malhotra, "A Diacidic Motif Determines Unconventional Secretion of Wild-Type and ALS-Linked Mutant SOD1," *Journal of Cell Biology* 216, no. 9 (2017): 2691–2700.

23. A. J. Curwin, K. Kurokawa, G. Bigliani, N. Brouwers, A. Nakano, and V. Malhotra, "The Pathway of Unconventional Protein Secretion Involves CUPS and a Modified Trans-Golgi Network," *Journal of Cell Biology* 224, no. 5 (2025): e202312120.

24. D. Cruz-Garcia, A. J. Curwin, J. F. Popoff, C. Bruns, J. M. Duran, and V. Malhotra, "Remodeling of Secretory Compartments Creates CUPS During Nutrient Starvation," *Journal of Cell Biology* 207, no. 6 (2014): 695–703.

25. D. Cruz-Garcia, N. Brouwers, V. Malhotra, and A. J. Curwin, "Reactive Oxygen Species Triggers Unconventional Secretion of Antioxidants and Acb1," *Journal of Cell Biology* 219, no. 4 (2020): e201905028.



26. H. Y. Gee, S. H. Noh, B. L. Tang, K. H. Kim, and M. G. Lee, "Rescue of  $\Delta F508$ -CFTR Trafficking via a GRASP-Dependent Unconventional Secretion Pathway," *Cell* 146, no. 5 (2011): 746–760.
27. H. Y. Gee, J. Kim, and M. G. Lee, "Unconventional Secretion of Transmembrane Proteins," *Seminars in Cell & Developmental Biology* 83 (2018): 59–66.
28. J. Meldolesi, "Unconventional Protein Secretion Dependent on Two Extracellular Vesicles: Exosomes and Ectosomes," *Frontiers in Cell and Development Biology* 10 (2022): 877344.
29. A. D. Senol, M. Samarani, S. Syan, et al., " $\alpha$ -Synuclein Fibrils Subvert Lysosome Structure and Function for the Propagation of Protein Misfolding Between Cells Through Tunneling Nanotubes," *PLoS Biology* 19, no. 7 (2021): e3001287, <https://pubmed.ncbi.nlm.nih.gov/34283825/>.
30. S. Abounit, J. W. Wu, K. Duff, G. S. Victoria, and C. Zurzolo, "Tunneling Nanotubes: A Possible Highway in the Spreading of Tau and Other Prion-Like Proteins in Neurodegenerative Diseases," *Prion* 10, no. 5 (2016): 344–351.
31. C. Zurzolo, "Tunneling Nanotubes: Reshaping Connectivity," *Current Opinion in Cell Biology* 71 (2021): 139–147.
32. M. Chiritoiu, N. Brouwers, G. Turacchio, M. Pirozzi, and V. Malhotra, "GRASP55 and UPR Control Interleukin-1 $\beta$  Aggregation and Secretion," *Developmental Cell* 49, no. 1 (2019): 145–155.e4.
33. X. Zhang, L. Wang, S. C. Ireland, et al., "GORASP2/GRASP55 Collaborates With the PtdIns3K UVRAG Complex to Facilitate Autophagosome-Lysosome Fusion," *Autophagy* 15, no. 10 (2019): 1787–1800, <https://doi.org/10.1080/15548627.2019.1596480>.
34. J. Nüchel, M. Tauber, J. L. Nolte, et al., "An mTORC1-GRASP55 Signaling Axis Controls Unconventional Secretion to Reshape the Extracellular Proteome Upon Stress," *Molecular Cell* 81, no. 16 (2021): 3275–3293.e12.
35. B. Tancini, S. Buratta, F. Delo, et al., "Lysosomal Exocytosis: The Extracellular Role of an Intracellular Organelle," *Membranes* 10, no. 12 (2020): 406.
36. S. Ghosh, T. A. Dellibovi-Ragheb, A. Kerviel, et al., " $\beta$ -Coronaviruses Use Lysosomes for Egress Instead of the Biosynthetic Secretory Pathway," *Cell* 183, no. 6 (2020): 1520–1535.e14.
37. Y. Xu, S. Du, J. A. Marsh, et al., "TFEB Regulates Lysosomal Exocytosis of Tau and Its Loss of Function Exacerbates Tau Pathology and Spreading," *Molecular Psychiatry* 26, no. 10 (2021): 5925–5939, <https://pubmed.ncbi.nlm.nih.gov/32366951/>.
38. D. L. Medina, A. Fraldi, V. Bouche, et al., "Transcriptional Activation of Lysosomal Exocytosis Promotes Cellular Clearance," *Developmental Cell* 21, no. 3 (2011): 421–430.
39. S. Abounit, L. Bousset, F. Loria, et al., "Tunneling Nanotubes Spread Fibrillar  $\alpha$ -Synuclein by Intercellular Trafficking of Lysosomes," *EMBO Journal* 35, no. 19 (2016): 2120–2138.
40. H. Cao, M. Sekiya, M. E. Ertunc, et al., "Adipocyte Lipid Chaperone aP2 Is a Secreted Adipokine Regulating Hepatic Glucose Production," *Cell Metabolism* 17 (2013): 768–778.
41. C. L. Evavold, J. Ruan, Y. Tan, S. Xia, H. Wu, and J. C. Kagan, "The Pore-Forming Protein Gasdermin D Regulates Interleukin-1 Secretion From Living Macrophages," *Immunity* 48 (2018): 35–44.e6.
42. L. Fourriere, S. Divoux, M. Roceri, F. Perez, and G. Boncompain, "Microtubule-Independent Secretion Requires Functional Maturation of Golgi Elements," *Journal of Cell Science* 129, no. 17 (2016): 3238–3250.
43. J. P. Steringer, S. Lange, S. Čujová, et al., "Key Steps in Unconventional Secretion of Fibroblast Growth Factor 2 Reconstituted With Purified Components," *eLife* 6 (2017): e28985.
44. R. Sitia and A. Rubartelli, "The Unconventional Secretion of IL-1 $\beta$ : Handling a Dangerous Weapon to Optimize Inflammatory Responses," *Seminars in Cell & Developmental Biology* 83 (2018): 12–21.
45. S. J. Popa, S. E. Stewart, and K. Moreau, "Unconventional Secretion of Annexins and Galectins," *Seminars in Cell & Developmental Biology* 83 (2018): 42–50.
46. S. Wu, N. C. Hernandez Villegas, D. W. Sirkis, I. Thomas-Wright, R. Wade-Martins, and R. Schekman, "Unconventional Secretion of  $\alpha$ -Synuclein Mediated by Palmitoylated DNAJC5 Oligomers," *eLife* 12 (2023): e85837.
47. P. Gosset, W. Camu, C. Raoul, and A. Mezghrani, "Prionoids in Amyotrophic Lateral Sclerosis," *Brain Communications* 4, no. 3 (2022): fcac145.
48. T. Katsinelos, M. Zeitler, E. Dimou, et al., "Unconventional Secretion Mediates the Trans-Cellular Spreading of Tau," *Cell Reports* 23, no. 7 (2018): 2039–2055.
49. T. Katsinelos, W. A. McEwan, T. R. Jahn, and W. Nickel, "Identification of Cis-Acting Determinants Mediating the Unconventional Secretion of Tau," *Scientific Reports* 11, no. 1 (2021): 12946, <https://doi.org/10.1038/s41598-021-92433-3>.
50. T. Azad, A. Tashakor, and S. Hosseinkhani, "Split-Luciferase Complementary Assay: Applications, Recent Developments, and Future Perspectives," *Analytical and Bioanalytical Chemistry* 406, no. 23 (2014): 5541–5560.
51. G. Boncompain, S. Divoux, N. Gareil, et al., "Synchronization of Secretory Protein Traffic in Populations of Cells," *Nature Methods* 9 (2012): 493–498.
52. Y. Misumi, Y. Misumi, K. Miki, A. Takatsuki, G. Tamura, and Y. Ikehara, "Novel Blockade by Brefeldin A of Intracellular Transport of Secretory Proteins in Cultured Rat Hepatocytes," *Journal of Biological Chemistry* 261 (1986): 11398–11403.
53. J. Lippincott-Schwartz, L. C. Yuan, J. S. Bonifacio, and R. D. Klausner, "Rapid Redistribution of Golgi Proteins Into the ER in Cells Treated With Brefeldin A: Evidence for Membrane Cycling From Golgi to ER," *Cell* 56, no. 5 (1989): 801–813.
54. G. A. Mardones, C. M. Snyder, and K. E. Howell, "Cis-Golgi Matrix Proteins Move Directly to Endoplasmic Reticulum Exit Sites by Association With Tubules," *Molecular Biology of the Cell* 17, no. 1 (2006): 525–538.
55. C. M. Carr and J. Rizo, "At the Junction of SNARE and SM Protein Function," *Current Opinion in Cell Biology* 22 (2010): 488–495.
56. M. Zhang, L. Liu, X. Lin, et al., "A Translocation Pathway for Vesicle-Mediated Unconventional Protein Secretion," *Cell* 181, no. 3 (2020): 637–652.e15.
57. Y. Sun, X. Tao, Y. Han, et al., "A Dual Role of ERGIC-Localized Rabs in TMED10-Mediated Unconventional Protein Secretion," *Nature Cell Biology* 26, no. 7 (2024): 1077–1092.
58. C. A. Brunello, M. Merezko, R. L. Uronen, and H. J. Huttunen, "Mechanisms of Secretion and Spreading of Pathological Tau Protein," *Cellular and Molecular Life Sciences* 77, no. 9 (2020): 1721–1744.
59. S. E. Stewart, S. A. Menzies, S. J. Popa, et al., "A Genome-Wide CRISPR Screen Reconciles the Role of N-Linked Glycosylation in Galectin-3 Transport to the Cell Surface," *Journal of Cell Science* 130 (2017): 3234–3247.
60. C. Tallon, K. R. Hollinger, A. Pal, et al., "Nipping Disease in the Bud: nSMase2 Inhibitors as Therapeutics in Extracellular Vesicle-Mediated Diseases," *Drug Discovery Today* 26, no. 7 (2021): 1656–1668.
61. L. Liu, M. Zhang, and L. Ge, "Protein Translocation Into the ERGIC: An Upstream Event of Secretory Autophagy," *Autophagy* 16, no. 7 (2020): 1358–1360.



62. S. Munro and H. R. Pelham, "A C-Terminal Signal Prevents Secretion of Luminal ER Proteins," *Cell* 48, no. 5 (1987): 899–907.
63. M. J. Lewis and H. R. Pelham, "Ligand-Induced Redistribution of a Human KDEL Receptor From the Golgi Complex to the Endoplasmic Reticulum," *Cell* 68, no. 2 (1992): 353–364.
64. R. Byström, P. M. Andersen, G. Gröbner, and M. Oliveberg, "SOD1 Mutations Targeting Surface Hydrogen Bonds Promote Amyotrophic Lateral Sclerosis Without Reducing Apo-State Stability," *Journal of Biological Chemistry* 285, no. 25 (2010): 19544–19552.
65. L. F. Barbosa, F. M. Cerqueira, A. F. A. Macedo, et al., "Increased SOD1 Association With Chromatin, DNA Damage, p53 Activation, and Apoptosis in a Cellular Model of SOD1-Linked ALS," *Biochimica et Biophysica Acta (BBA) - Molecular Basis of Disease* 1802, no. 5 (2010): 462–471.
66. S. Pedrini, D. Sau, S. Guareschi, et al., "ALS-Linked Mutant SOD1 Damages Mitochondria by Promoting Conformational Changes in Bcl-2," *Human Molecular Genetics* 19, no. 15 (2010): 2974–2986.
67. V. Khurana, Y. Lu, M. L. Steinhilb, S. Oldham, J. M. Shulman, and M. B. Feany, "TOR-Mediated Cell-Cycle Activation Causes Neurodegeneration in a *Drosophila* Tauopathy Model," *Current Biology* 16, no. 3 (2006): 230–241.
68. G. T. Bramblett, M. Goedert, R. Jakes, S. E. Merrick, J. Q. Trojanowski, and V. M. Lee, "Abnormal Tau Phosphorylation at Ser396 in Alzheimer's Disease Recapitulates Development and Contributes to Reduced Microtubule Binding," *Neuron* 10, no. 6 (1993): 1089–1099.
69. Y. Talmat-Amar, Y. Arribat, C. Redt-Clouet, et al., "Important Neuronal Toxicity of Microtubule-Bound Tau In Vivo in *Drosophila*," *Human Molecular Genetics* 20, no. 19 (2011): 3738–3745.
70. I. Grundke-Iqbal, K. Iqbal, Y. C. Tung, M. Quinlan, H. M. Wisniewski, and L. I. Binder, "Abnormal Phosphorylation of the Microtubule-Associated Protein Tau (Tau) in Alzheimer Cytoskeletal Pathology," *Proceedings of the National Academy of Sciences of the United States of America* 83, no. 13 (1986): 4913–4917.
71. D. M. Lopez, C. J. Maltby, H. Warming, et al., "A Luminescence-Based Reporter to Study Tau Secretion Reveals Overlapping Mechanisms for the Release of Healthy and Pathological Tau," *Frontiers in Neuroscience* 17 (2023): 1196007.
72. N. R. Barthélemy, B. Saef, Y. Li, et al., "CSF Tau Phosphorylation Occupancies at T217 and T205 Represent Improved Biomarkers of Amyloid and Tau Pathology in Alzheimer's Disease," *Nature Aging* 3, no. 4 (2023): 391–401.
73. A. D. Sperfeld, M. B. Collatz, H. Baier, et al., "FTDP-17: An Early-Onset Phenotype With Parkinsonism and Epileptic Seizures Caused by a Novel Mutation," *Annals of Neurology* 46, no. 5 (1999): 708–715.
74. M. Goedert, R. Jakes, and R. A. Crowther, "Effects of Frontotemporal Dementia FTDP-17 Mutations on Heparin-Induced Assembly of Tau Filaments," *FEBS Letters* 450, no. 3 (1999): 306–311.
75. C. W. Cotman, W. W. Poon, R. A. Rissman, and M. Blurton-Jones, "The Role of Caspase Cleavage of Tau in Alzheimer Disease Neuropathology," *Journal of Neuropathology and Experimental Neurology* 64, no. 2 (2005): 104–112.
76. A. L. Guillozet-Bongaarts, F. Garcia-Sierra, M. R. Reynolds, et al., "Tau Truncation During Neurofibrillary Tangle Evolution in Alzheimer's Disease," *Neurobiology of Aging* 26, no. 7 (2005): 1015–1022.
77. A. L. Guillozet-Bongaarts, M. E. Cahill, V. L. Cryns, M. R. Reynolds, R. W. Berry, and L. I. Binder, "Pseudophosphorylation of Tau at Serine 422 Inhibits Caspase Cleavage: In Vitro Evidence and Implications for Tangle Formation In Vivo," *Journal of Neurochemistry* 97, no. 4 (2006): 1005–1014.
78. C. Bellenguez, F. Küçükali, I. E. Jansen, et al., "New Insights Into the Genetic Etiology of Alzheimer's Disease and Related Dementias," *Nature Genetics* 54, no. 4 (2022): 412–436.
79. K. Satoh, S. Abe-Dohmae, S. Yokoyama, P. St George-Hyslop, and P. E. Fraser, "ATP-Binding Cassette Transporter A7 (ABCA7) Loss of Function Alters Alzheimer Amyloid Processing," *Journal of Biological Chemistry* 290, no. 40 (2015): 24152–24165.
80. R. Bhattacharyya, C. A. F. Teves, A. Long, M. Hofert, and R. E. Tanzi, "The Neuronal-Specific Isoform of BIN1 Regulates  $\beta$ -Secretase Cleavage of APP and A $\beta$  Generation in a RIN3-Dependent Manner," *Scientific Reports* 12 (2022): 3486.
81. O. M. Andersen, J. Reiche, V. Schmidt, et al., "Neuronal Sorting Protein-Related Receptor sorLA/LR11 Regulates Processing of the Amyloid Precursor Protein," *Proceedings of the National Academy of Sciences of the United States of America* 102, no. 38 (2005): 13461–13466.
82. M. S. Wolfe, W. Xia, B. L. Ostaszewski, T. S. Diehl, W. T. Kimberly, and D. J. Selkoe, "Two Transmembrane Aspartates in Presenilin-1 Required for Presenilin Endoproteolysis and Gamma-Secretase Activity," *Nature* 398, no. 6727 (1999): 513–517.
83. T. C. M. Seegar, L. B. Killingsworth, N. Saha, et al., "Structural Basis for Regulated Proteolysis by the  $\alpha$ -Secretase ADAM10," *Cell* 171, no. 7 (2017): 1638–1648.e7.
84. Q. Xiao, S. C. Gil, P. Yan, et al., "Role of Phosphatidylinositol Clathrin Assembly Lymphoid-Myeloid Leukemia (PICALM) in Intracellular Amyloid Precursor Protein (APP) Processing and Amyloid Plaque Pathogenesis," *Journal of Biological Chemistry* 287, no. 25 (2012): 21279–21289, <https://pubmed.ncbi.nlm.nih.gov/22539346/>.
85. F. Eysert, A. Coulon, E. Boscher, et al., "Alzheimer's Genetic Risk Factor FERMT2 (Kindlin-2) Controls Axonal Growth and Synaptic Plasticity in an APP-Dependent Manner," *Molecular Psychiatry* 26, no. 10 (2021): 5592–5607.
86. S. Kim, H. Chun, Y. Kim, et al., "Astrocytic Autophagy Plasticity Modulates A $\beta$  Clearance and Cognitive Function in Alzheimer's Disease," *Molecular Neurodegeneration* 19, no. 1 (2024): 55.
87. M. K. Eccles, N. Main, R. Carlessi, et al., "Quantitative Comparison of Presenilin Protein Expression Reveals Greater Activity of PS2- $\gamma$ -Secretase," *FASEB Journal* 38, no. 1 (2024): e23396.
88. Y. Li, D. Liu, X. Zhang, S. Rimal, B. Lu, and S. Li, "RACK1 and IRE1 Participate in the Translational Quality Control of Amyloid Precursor Protein in *Drosophila* Models of Alzheimer's Disease," *Journal of Biological Chemistry* 300, no. 3 (2024): 105719.
89. M. P. Szabo, S. Mishra, A. Knupp, and J. E. Young, "The Role of Alzheimer's Disease Risk Genes in Endolysosomal Pathways," *Neurobiology of Disease* 162 (2022): 105576.
90. K. Ando, S. Nagaraj, F. Küçükali, et al., "PICALM and Alzheimer's Disease: An Update and Perspectives," *Cells* 11, no. 24 (2022): 3994.
91. C. Hung, E. Tuck, V. Stubbs, et al., "SORL1 Deficiency in Human Excitatory Neurons Causes APP-Dependent Defects in the Endolysosome-Autophagy Network," *Cell Reports* 35, no. 11 (2021): 109259.
92. J. Hardy and D. J. Selkoe, "The Amyloid Hypothesis of Alzheimer's Disease: Progress and Problems on the Road to Therapeutics," *Science* 297, no. 5580 (2002): 353–356, <https://pubmed.ncbi.nlm.nih.gov/12130773/>.
93. R. A. Nixon and D. C. Rubinsztein, "Mechanisms of Autophagy-Lysosome Dysfunction in Neurodegenerative Diseases," *Nature Reviews. Molecular Cell Biology* 25, no. 11 (2024): 926–946.
94. I. Annunziata, A. Patterson, D. Helton, et al., "Lysosomal NEU1 Deficiency Affects Amyloid Precursor Protein Levels and Amyloid- $\beta$  Secretion via Deregulated Lysosomal Exocytosis," *Nature Communications* 4 (2013): 2734.
95. C. L. Masters and K. Beyreuther, "Alzheimer's Centennial Legacy: Prospects for Rational Therapeutic Intervention Targeting the Abeta Amyloid Pathway," *Brain* 129, no. Pt 11 (2006): 2823–2839.

96. H. Chung, M. I. Brazil, T. T. Soe, and F. R. Maxfield, "Uptake, Degradation, and Release of Fibrillar and Soluble Forms of Alzheimer's Amyloid Beta-Peptide by Microglial Cells," *Journal of Biological Chemistry* 274, no. 45 (1999): 32301–32308.
97. R. G. Jacquet, F. G. Ibáñez, K. Picard, et al., "Microglia Degrade Alzheimer's Amyloid-Beta Deposits Extracellularly via Digestive Exophagy," *Cell Reports* 43, no. 12 (2024): 115052.
98. D. Cruz-Garcia, V. Malhotra, and A. J. Curwin, "Unconventional Protein Secretion Triggered by Nutrient Starvation," *Seminars in Cell & Developmental Biology* 83 (2018): 22–28.
99. L. Liu, L. Zhang, X. Hao, et al., "Coronavirus Envelope Protein Activates TMED10-Mediated Unconventional Secretion of Inflammatory Factors," *Nature Communications* 15, no. 1 (2024): 8708.
100. Y. Wang, M. Huang, X. Mu, et al., "TMED10-Mediated Unconventional Secretion of IL-33 Regulates Intestinal Epithelium Differentiation and Homeostasis," *Cell Research* 34, no. 3 (2024): 258–261.
101. M. Goedert, M. Masuda-Suzukake, and B. Falcon, "Like Prions: The Propagation of Aggregated Tau and  $\alpha$ -Synuclein in Neurodegeneration," *Brain* 140, no. 2 (2017): 266–278.
102. A. Mudher, M. Colin, S. Dujardin, et al., "What Is the Evidence That Tau Pathology Spreads Through Prion-Like Propagation?," *Acta Neuropathologica Communications* 5, no. 1 (2017): 99.
103. S. Padmanabhan, M. R. Biswal, R. Manjithaya, and M. K. Prakash, "Exploring the Context of Diacidic Motif DE as a Signal for Unconventional Protein Secretion in Eukaryotic Proteins," *Wellcome Open Research* 3 (2018): 148.
104. C. Semino, S. Carta, M. Gattorno, R. Sitia, and A. Rubartelli, "Progressive Waves of IL-1 $\beta$  Release by Primary Human Monocytes via Sequential Activation of Vesicular and Gasdermin D-Mediated Secretory Pathways," *Cell Death & Disease* 9, no. 11 (2018): 1088.
105. A. Lopez, F. H. Siddiqi, J. Villeneuve, et al., "Carbonic Anhydrase Inhibition Ameliorates Tau Toxicity via Enhanced Tau Secretion," *Nature Chemical Biology* 21 (2025): 577–587.
106. J. M. Long and D. M. Holtzman, "Alzheimer Disease: An Update on Pathobiology and Treatment Strategies," *Cell* 179, no. 2 (2019): 312–339.
107. Y. Tanaka, K. Yamada, K. Satake, et al., "Seeding Activity-Based Detection Uncovers the Different Release Mechanisms of Seed-Competent Tau Versus Inert Tau via Lysosomal Exocytosis," *Frontiers in Neuroscience* 13 (2019): 1258.
108. E. Ahat, S. Bui, J. Zhang, et al., "GRASP55 Regulates the Unconventional Secretion and Aggregation of Mutant Huntingtin," *Journal of Biological Chemistry* 298, no. 8 (2022): 102219, <https://doi.org/10.1016/j.jbc.2022.102219>.
109. E. J. Bae, M. Choi, J. T. Kim, et al., "TNF- $\alpha$  Promotes  $\alpha$ -Synuclein Propagation Through Stimulation of Senescence-Associated Lysosomal Exocytosis," *Experimental & Molecular Medicine* 54, no. 6 (2022): 788–800.
110. Y. X. Xie, N. N. Naseri, J. Fels, et al., "Lysosomal Exocytosis Releases Pathogenic  $\alpha$ -Synuclein Species From Neurons in Synucleinopathy Models," *Nature Communications* 13, no. 1 (2022): 4918.
111. X. Zhao, Y. Guan, F. Liu, et al., "SNARE Proteins Mediate  $\alpha$ -Synuclein Secretion via Multiple Vesicular Pathways," *Molecular Neurobiology* 59, no. 1 (2022): 405–419.

## Supporting Information

Additional supporting information can be found online in the Supporting Information section.